RESTING STATE BRAIN CONNECTIVITY VIA BICOHERENCE AND
COHERENCE

A THESIS SUBMITTED TO

THE GRADUATE SCHOOL OF INFORMATICS OF

MIDDLE EAST TECHNICAL UNIVERSITY

BY

AHMET LEVENT KANDEMİR

IN PARTIAL FULFILLMENT OF THE REQUIREMENTS FOR THE DEGREE OF

MASTER OF SCIENCE

IN

MEDICAL INFORMATICS

MARCH 2018

RESTING STATE BRAIN CONNECTIVITY VIA BICOHERENCE AND COHERENCE

Submitted by AHMET LEVENT KANDEMİR in partial fulfillment of the requirements for the degree of **Master of Science in Medical Informatics Department, Middle East Technical University** by,

Prof. Dr. Deniz Zeyrek Bozşahin
Dean, **Graduate School of Informatics** _____

Assoc. Prof. Dr. Yeşim Aydın Son
Head of Department, **Health Informatics** _____

Assoc. Prof. Dr. Tolga Esat Özkurt
Supervisor, **Health Informatics Dept., METU** _____

Examining Committee Members:

Prof. Dr. Ünal Erkan Mumcuoğlu
Health Informatics Dept., METU _____

Assoc. Prof. Dr. Tolga Esat Özkurt
Health Informatics Dept., METU _____

Assist. Prof. Dr. Murat Perit Çakır
Cognitive Science Dept., METU _____

Assist. Prof. Dr. Tolga Çukur
Electrical and Electronics Engineering Dept., Bilkent University _____

Assoc. Prof. Dr. Yeşim Aydın Son
Health Informatics Dept., METU _____

Date: _____21.03.2018_____

I hereby declare that all information in this document has been obtained and presented in accordance with academic rules and ethical conduct. I also declare that, as required by these rules and conduct, I have fully cited and referenced all material and results that are not original to this work.

Name, Last Name: AHMET LEVENT KANDEMİR

Signature   : _____

ABSTRACT

RESTING STATE BRAIN CONNECTIVITY VIA BICOHERENCE AND
COHERENCE

Kandemir, Ahmet Levent

MSc., Department of Medical Informatics

Supervisor: Assoc. Prof. Dr. Tolga Esat Özkurt

March 2018, 54 pages

The human brain is a complex and dynamical system, which consists of segregated areas specialized for perceptual or motor processing. Task-specific functions are only carried out by integration of these segregated regions. Thus, in order to understand the human brain, it is very important to understand underlying network structure. There are various metrics to investigate the brain connectivity and each day, new metrics are introduced in the field. This study concentrates on bicoherence analysis. Bicoherence is a third order spectral coupling measure which is used to investigate nonlinear interactions, particularly quadratic phase coupling, within the brain. High computational cost and being prone to volume conduction effect has made bicoherence impractical in neuroscience. New approaches to bicoherence promise reduction in computational cost and robustness to volume conduction. 'Sliced Bicoherence' is a bicoherence metric calculating only the main diagonal of the bicoherence matrix with a significant reduction in calculation time. Sufficiency of calculation of only the main diagonal of the matrix has been an open question about the subject. On the other hand, newly introduced 'Subtracted Bicoherence' is an improvement over 'Sliced Bicoherence', eliminating volume conduction. Within the scope of this study, it was shown that the information content of bicoherence matrix was concentrated on the main diagonal. Also, validity and usability of 'Sliced Bicoherence' and 'Subtracted Bicoherence' in connectivity analysis were demonstrated by comparing them to well known 'Coherence' and 'Imaginary Coherency' metrics.

Keywords: bicoherence, coherence, connectivity, cross-frequency coupling, resting state MEG analysis

iv

ÖZ

UYUMLULUK VE İKİZ-UYUMLULUK ARACILIĞIYLA DİNLENME HALİ BAĞLANTISALLIK ANALİZİ

Kandemir, Ahmet Levent

Yüksek Lisans, Sağlık Bilişimi Bölümü

Tez Yöneticisi: Doç. Dr. Tolga Esat Özkurt

Mart 2018, 54 sayfa

İnsan beyni algısal ve motor faaliyetler üzerine özelleşmiş, ayrık bölgelerden oluşan karmaşık ve dinamik bir yapıdır. Beyin faaliyetleri ancak bu ayrık bölgelerin bütünleşmesiyle gerçekleştirilebilir. Bu nedenle, insan beynini anlayabilmek için öncelikli olarak altta yatan ağ yapısını anlamak gerekir. Literatürde beyin içerisinde bağlantısallık analizi gerçekleştirmek üzere geliştirilmiş bir çok metot bulunmaktadır ve her gün yeni metotlar bu arşive eklenmektedir. Bu çalışma, ikiz-uyumluluk üzerine yoğunlaşmıştır. İkiz-uyumluluk, doğrusal olmayan etkileşimleri, özellikle Karesel Faz Eşleşmelerini, araştırmak için kullanılan üçüncü derece izgesel eşleşme ölçüsüdür. İkiz-uyumluluk yüksek hesaplama maliyeti ve hacimsel iletkenlik nedeniyle sinirbilim alanında bugüne kadar çok kullanışlı olamamıştır. Yeni yaklaşımlar hesaplama maliyetinde düşüşü ve hacimsel iletkenliğe dayanıklılığı vadetmektedir. 'İkiz-Uyumluluk Dilimi' sadece ana köşegeni hesaplayan ve hesaplama zamanını ciddi bir şekilde düşüren ikiz-uyumluluk tabanlı bir ölçüdür. Sadece ana köşegen hesabının yeterliliği tartışmaya açıktır. Öte yandan, yeni önerilen 'Çıkarılmış İkiz-Uyumluluk', 'İkiz-Uyumluluk Dilimi'ne getirilen bir geliştirmedir ve hacimsel iletkenliği ortadan kaldırmaktadır. Bu çalışma kapsamında, ikiz-uyumluluk matrisinin bilgi içeriğinin ana köşegen üzerinde toplandığını gösterilmektedir. Ayrıca, 'İkiz-Uyumluluk Dilimi' ve 'Çıkarılmış İkiz-Uyumluluk' metotlarının geçerliliğini ve bağlantısallık analizinde kullanılabilirliğini bu metotların literatürde iyi bilinen Uyumluluk ve Sanal Uyumluluk metotlarıyla kıyaslanmasıyla kanıtlanmaktadır.

Anahtar Sözcükler: ikiz-uyumluluk, uyumluluk, bağlantısallık, çapraz-frekans analizi, dinlenme hali MEG analizi

To my family, may it grow bigger as the years pass by…

ACKNOWLEDGMENTS

First of all, I would like to thank my supervisor, Assoc. Prof. Dr. Tolga Esat Özkurt for giving me opportunity to work in this project, for believing in me and encouraging me throughout my studies. He was always patient, understanding and helpful.

I would like to thank my colleagues both at the university and in my company. They always supported my work, helped at times of need and encouraged me to make that extra mile.

I would also like to thank my family, for their unconditional love and support. I could not make it here without them.

And last but not least, I would like to thank my wife, for putting up with me in times of worry, exhaustion and boredom, for supporting me and being there for me whenever I needed throughout this thesis. She made everything easier and tolerable.

TABLE OF CONTENTS

LIST OF TABLES

LIST OF FIGURES

LIST OF ABBREVIATIONS

AAL	Automated Anatomic Labelling
AVOI	Anatomical Volume of Interest
BEM	Boundary Element Model
BOLD	Blood Oxygen Level-Dependent
DICS	Dynamic Imaging of Coherent Sources
ECG	Electrocardiography
ECD	Equivalent Current Dipoles
EEG	Electroencephalography
EOG	Electrooculography
FEM	Finite Element Model
fMRI	Magnetic Resonance Imaging
HCP	Human Connectome Project
HOSA	Higher Order Spectral Analysis
ICA	Independent Component Analysis
LCMV	Linearly Constrained Minimum-Variance Beamforming
MEG	Magnetoencephalography
MUSIC	Multiple Signal Classification
MRI	Magnetic Resonance Imaging
PCA	Principal Component Analysis
QPC	Quadratic Phase Coupling
SQUID	Superconducting Quantum Interference Device
SAM	Synthetic Aperture Magnetometry

CHAPTER 1

INTRODUCTION

Understanding human brain has been one of the greatest challenges of our conquest to understanding ourselves. In general, the multidisciplinary study of brain and nervous system is called Neuroscience. The earliest Neuroscience studies date back to ancient Egypt. The first description of the word 'brain' is found in The Edwin Smith Surgical Papyrus (Mohamed, 2008).The papyrus is based on texts from 3000 BC and it gives information about 48 different types of brain injuries and treatment methods (Feldman & Goodrich, 1999). Nonetheless, it was not until the Ancient Greeks for the seat of intelligence to be stated as the brain (Gross C. G., 1987). Galen (129 AD-199 AD) of Roman Empire was a great contributor to the field. He was the leading physician of his time and he demonstrated many functions of the nervous system (Freemon, 1994). Even though the scientific enlightenment about the human brain slowed down during the medieval era, the greatest discoveries were to be made during the 16th century. Andreas Vesalius (1514-1564), a follower of Galen, identified many structural parts of both the brain and the nervous system through dissections of human cadavers (Van Laere, 1993). He was later to be known as the founder of modern anatomy. Later on, as the technology developed and the knowledge about the field increased, neuroimaging techniques paved the way for greater discoveries.

Electroencephalography (EEG) along with Magnetoencephalography (MEG), and Magnetic Resonance Imaging (MRI) are some of the most important neuroimaging modalities used in modern neuroscience. First human EEG was recorded by Hans Berger in 1924 (Haas, 2003) and since then, EEG still remains the most widely used functional test allowing to directly monitor electrical correlates of neural function with high temporal resolution (He, Yang, Wilke, & Yuan, 2011). While EEG measures the electrical activity of neural firing, MEG measures the magnetic fields generated by accumulated postsynaptic potentials. MEG is an alternative to EEG developed by David Cohen in 1968 with the main advantage of better spatial resolution in locating cortical events (Hämäläinen, Hari, Ilmoniemi, Knuutila, & Lounasmaa, 1993). Together with the use of MRI, EEG/MEG recordings can be mapped to subject specific geometric models, making better assumptions thanks to anatomical information (Liu, Ding, & He, 2006).

With the good establishment of neuroimaging techniques, a new field of neuroscience emerged: the brain connectivity. The brain connectivity analysis is the study of anatomical links (structural connectivity), statistical dependencies (functional connectivity) and causal interactions (effective connectivity) between neurons and/or neuronal populations (Sporns, Brain Connectivity, 2007). This study concentrates on functional connectivity, which is described as the integration of segregated brain areas to operate as a network in several task-related and resting state activations. Functional

connectivity can be quantified with measures of statistical dependencies, such as correlations or coherence (Friston K. , 2011). Functional connectivity investigates oscillatory synchronization between distinct brain regions which has been proven useful to evaluate functioning of pathological and normal brain (Schnitzler & Gross, 2005; Siegel, Donner, & Engel, 2012).

Functional connectivity may be investigated in means of both linear and nonlinear interactions. Linear interactions within the brain are well studied using the measure of coherence. But linear approaches have limitations since the brain is evaluated as a nonlinear, dynamical system (Aydore, Pantazis, & Leahy, 2013). Thus, various phase estimation and cross-frequency measures are used frequently to investigate functional connectivity caused by nonlinear systems (Jirsa & Müller, 2013; Özkurt & Schnitzler, 2011; Florin & Baillet, 2015; Colclough, et al., 2016).

A subtype of nonlinear interactions, named quadratic phase coupling (QPC) is an interaction of three frequencies; f_1, f_2 and $f_1 + f_2$. In order to suggest a QPC interaction, sum of the phases at $f_1(\phi_1)$ and $f_2(\phi_2)$ should be the phase at frequency $f_1 + f_2$ $(\phi_1 + \phi_2)$ (Venkatakrishnan, Sukanesh, & Sangeetha, 2011). Bicoherence is a powerful tool to detect QPC and has been applied successfully to evaluate QPC types of nonlinear effects in human EEG and MEG (Barnett, Johnson, Naitoh, Hicks, & Nute, 1971; Dumermuth, Huber, Kleiner, & Gasser, 1971; Nikias & Mendel, 1993). Although proven useful, bicoherence has not found wide field of use in connectivity analysis due to heavy computational cost (Özkurt T. E., 2016). A pairwise bicoherence analysis of multivariate source data requires estimates in the order of $\sim N^2 x\ M^2$, where N and M denote the number of channels/sources and the number of sampled frequencies, respectively. There have been significant attempts to reduce the computational costs. Chella et al. (2014), used principal component analysis prior to source localization, reducing the number of channels to only principal components. On the other hand, Özkurt (2016) suggested an indirect estimation method, called 'sliced bicoherence', for calculating only the main diagonal of the bicoherence matrix for each pair of source data.

Aims of the Study

This study examines information content of the bicoherence matrix on resting state data and evaluates the efficiency of 'sliced bicoherence' and 'subtracted bicoherence'. A comparison between linear and nonlinear connectivity measures are also carried out in means of correlation estimation, volume conduction and reliability.

This thesis is comprised of 5 chapters including the introduction. The rest of the thesis is organized as follows: in the 2nd chapter, human brain, connectivity types and analysis will be described in detail. Detailed information on bispectral analysis and bicoherence will be provided. Materials and methods used in this study will be described in the 3rd chapter. Results and Discussions will be given in chapters 4 and 5, respectively.

CHAPTER 2

LITERATURE REVIEW

2.1   Human Brain and Connectivity

The human brain is an extremely complicated network composed of more than 10^{10} neurons. Each and every neuron in the brain has a special role in information processing and from a macro scale, each group of neurons specializes in performing special tasks. The idea of segregated areas specialized in specific functions was dominant during the 19th century. With the formulation of phrenology by Gall, the identification of specific functional brain regions gained attention in neuroscience as it can be seen from Figure 2.1 (Friston K. , 2011). Even though the idea was evaluated non-scientific and controversial at the time, further studies affirmed segregation of functional brain regions in a similar, yet different way. Taking anatomical connections between distant regions into consideration, it was realized that assigning a special function to a segregated area was not a realistic model. Instead, studies suggested that brain regions were actually specialized for perceptual or motor processing and task specific functions could only be carried out by integration of these segregated regions (Friston K. , 2011). Important contributions to the field were later made by Paul Broca, Eduart Hitzig, Gustav Fritsch, and Sir David Ferrier (Finger, 2000).
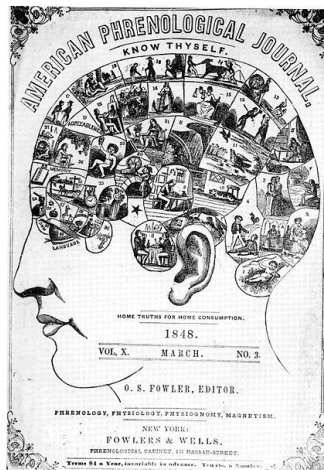
Figure 2.1: The Phrenological Chart. Front cover of The American Phrenological Journal: (1846 - Vol. 10, No. 3). [1]

---

[1] Figure from *http://en.wikipedia.org/wiki/Phrenology*

In the early twentieth century, more convincing evidence on the segregation of brain regions was discovered by anatomists Oscar Vogt, Cecile Vogt, Alfred Walter Campbell, and Korbinian Brodmann (Finger, 2000). The discoveries showed different characteristics of neuron groups localized at different regions of the brain (Figure 2.2) (Garey , 2006).
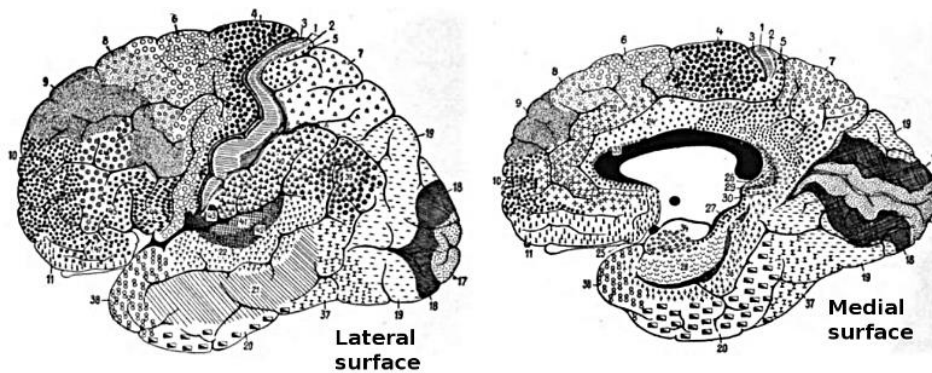
Figure 2.2: Brodmann's Cortex Classification. Brodmann split the cortex into 52 different areas based on the cytoarchitectural organization of neurons (Brodmann, 1909).[2]

All of the studies describing different characteristics of neurons starts with the most important breakthrough in neuroscience known as the neuron doctrine (Pawela & Biswal, 2011). The neuron theory was developed by Santiago Ramón y Cajal based on his extensive work on the details of neuron (López-Muñoz, Boya, & Alamo, 2006). His detailed illustrations of cellular connections in the brain form the basis of the field and may be considered as the beginning of the connectivity research (Figure 2.3) (Pawela & Biswal, 2011).
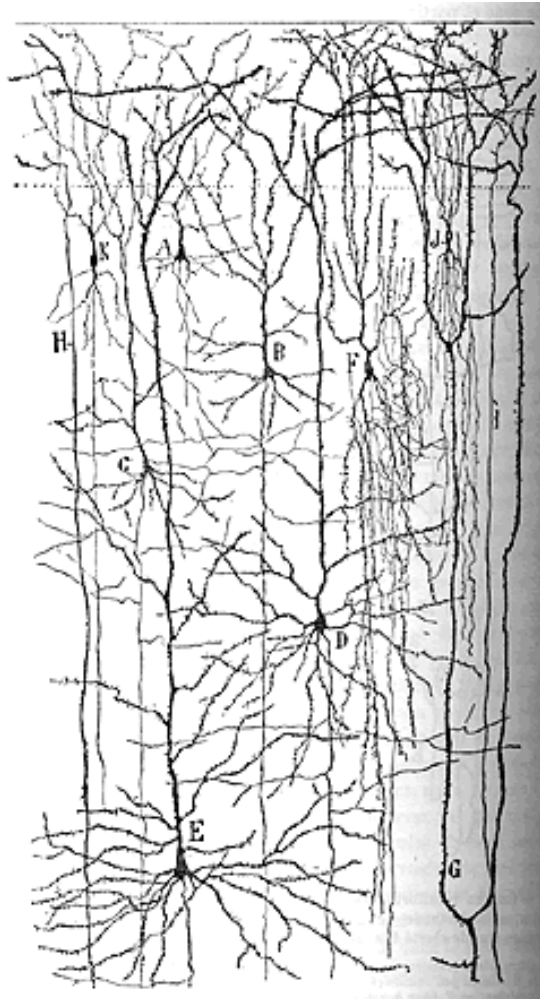
Figure 2.3: Superficial Layers of Human Frontal Cortex. Original drawings by Cajal on the basis of Golgi impregnation. Pyramidal (A, B, C, D, E) and non-pyramidal neurons (F, K) are visualized in detail[3].

2.1.1   Brain Connectivity

Brain connectivity has become one of the hot topics in neuroscience within the last few decades. Each year, new scientists from different fields join and the number of publications rises significantly. Figure 2.4 shows the number of publications in ScienceDirect (Elsevier) database for the last 5 years including the term 'brain connectivity'. New methods for connectivity analysis are introduced to the literature each year and scientists all around the world implement these methods to understand brain mechanisms to a greater extent.

---

[3] Figure from (Garcia-Lopez, Garcia-Marin, & Freire, 2010)
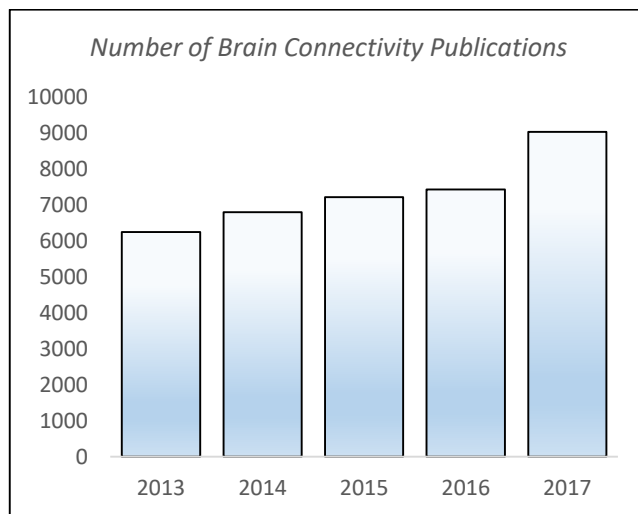
Figure 2.4: Brain Connectivity Publications. A significant increase in the interest for brain connectivity is observed[4].

Connectivity research is concentrated on anatomical pathways, interactions, and communication between distinct units (Pawela & Biswal, 2011). In a highly evolved nervous system, connectivity is described in 3 levels (Figure 2.5) (Sporns, Tononi, & Kötter, 2005);

Microscale: Microscale connectivity is described as the individual connections between individual neurons. Microscale is the fundamental neural connection type observed in all forms of life.

Mesoscale: Mesoscale connectivity describes networks of columns connecting neuronal populations.

Macroscale: Macroscale connectivity is the connection between distinct regions of the brain. At macroscale, pathways between larger neuronal populations are formed and complex functional networks are created.

In the literature, the term 'brain connectivity', although not limited, mostly refers to macroscale connectivity. Connectivity between distinct regions of the brain is of utmost interest. The remainder of the thesis will focus on macroscale connectivity and its importance in the field.

---

[4] Figure from *https://www.sciencedirect.com*
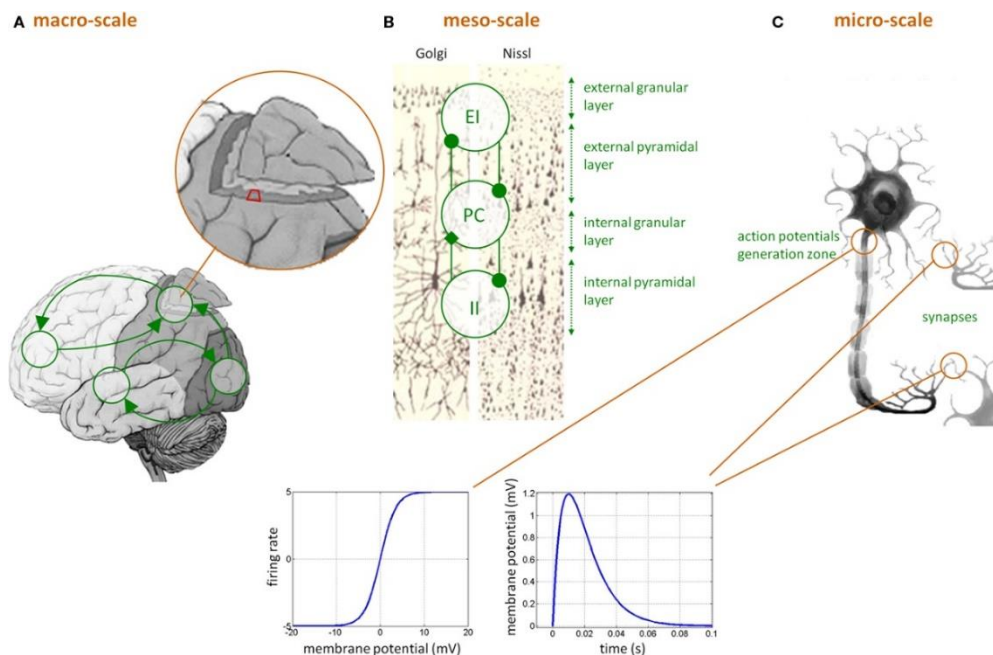
Figure 2.5: Levels of Connectivity. Different levels of brain connectivity is visualized in detail[5].

Apart from different levels, brain connectivity is also represented in three different types. These types investigate anatomical links (anatomical connectivity), statistical dependencies (functional connectivity) or causal interactions (effective connectivity) between distinct units within a nervous system (Sporns, 2007).

Anatomical Connectivity: Anatomical connectivity, also called structural connectivity, forms the *connectome* (Sporns, Tononi, & Kötter, 2005). Anatomical connectivity points to the presence of a physical connection between separate regions in the brain and describes the nature of the pathways (Hagmann, et al., 2008). The set of pathways in the brain is called white matter and latest observations suggest that anatomical connectivity may change over time substantially due to learning related plasticity of the white matter (Sampaio-Baptista & Johansen-Berg, 2017).

Functional Connectivity: Functional connectivity investigates two principal concepts: functional segregation and functional integration (Tononi, Sporns, & Edelman, 1994). Functional segregation is grouping of functionally specialized neurons into spatially distant brain regions. On the other hand, functional integration is the necessary communication between segregated areas in a task specific function (Duda, 2010). Functional connectivity is a statistical concept and examines statistical dependences between separate neuron populations (Sporns, 2007). Statistical dependence may be estimated by measuring interactions via several methods

---

[5] Figure from (Lemieux, Daunizeau, & Walker, 2011)

introduced to the literature within the last few decades. It is important to note that functional connectivity is not concerned about the structural link between spatially distant regions and the direction of the interaction.

Effective Connectivity: Effective connectivity describes the causal influences between neuron populations (Friston K. J., 1994). Effective connectivity is not only concerned with the communication between distant regions in the brain but it is also concerned with the direction of the communication (Sporns, 2007). Effective connectivity is observed through time series analysis since causality creates a time delay between activations of different brain regions.

Formally, brain connectivity patterns are represented in graph or matrix format. Figure 2.6 shows differences between types of connectivity. The remainder of this thesis concentrates on functional connectivity and discusses the methods developed to analyze it.
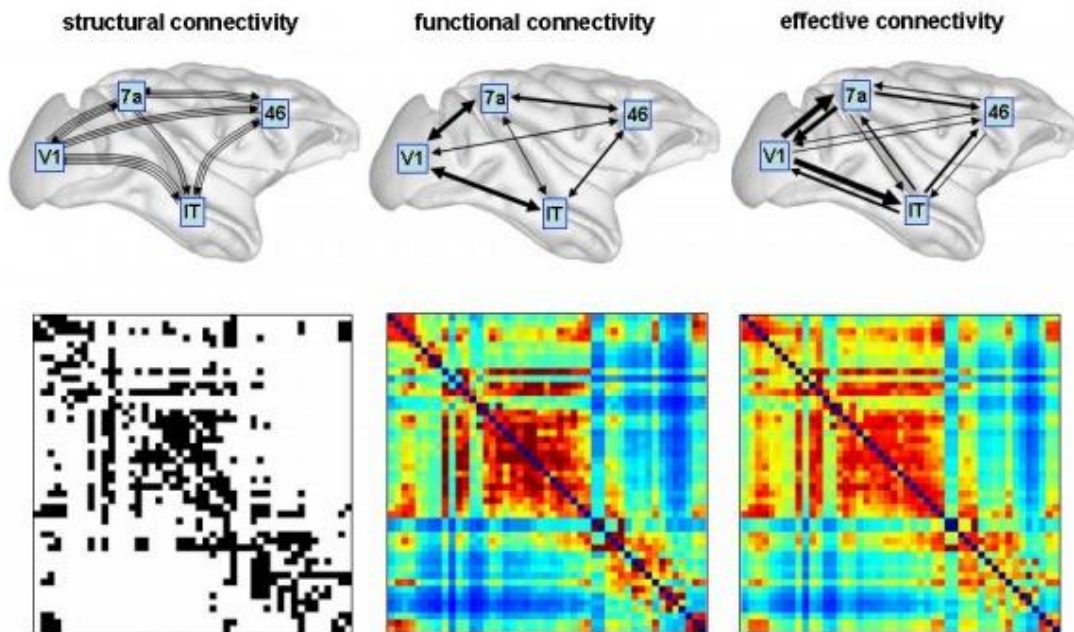
Figure 2.6: Types of Connectivity. Structural, functional and effective connectivity in macaque cortex. Bottom matrices represent binary connections for each type of connectivity[6].

---

[6] Figure from (Sporns, Brain Connectivity, 2007)

2.2   Investigating Functional Brain Connectivity

The first step in connectivity investigation is data acquisition. Apart from anatomical image acquisition, which is typically made with MRI, functional data should also be collected. With the recent advancements in technology, functional Magnetic Resonance Imaging (fMRI), EEG and MEG became the most frequently used modalities for connectivity analysis. After data acquisition, one has to solve forward-inverse problems to localize source activity.

2.2.1   Neuroimaging Modalities

Functional Magnetic Resonance Imaging (fMRI)

As soon as a neuron gets active, it needs energy to pump ions to return to the original state of polarization. This energy source is mostly covered by glucose. Since the brain does not store glucose, blood rushes to the site of activation, to transport glucose and oxygen in the form of oxy-hemoglobin. Due to magnetic properties of oxy-hemoglobin and deoxy-hemoglobin (Pauling & Coryell, 1936), the oxygenation concentration of blood alters the MRI signal. Researchers used these properties of hemoglobin to measure what would be later called as the blood oxygen level-dependent (BOLD) signal (Bandettini, Wong, Hinks, Tikofsky, & Hyde, 1992; Kwong, et al., 1992; Ogawa, et al., 1992). The basic principle of BOLD signal is that as the oxygen level of the blood increases, the noise in the MRI signal decreases and as a result, the signal quality increases (Ogawa, et al., 1992; Kwong, et al., 1992). This quality change in the MRI signal due to neuronal activity is called the hemodynamic response. Active regions of the brain appear brighter in the fMRI reaching the peak brightness at around 5s after the stimulus during a task specific experiment. Although this lag in response time reduces temporal resolution of fMRI, high spatial resolution of millimeters makes it one of the most important neuroimaging modalities used in neuroscience (Glover, 2011; Wallisch, 2014).

Electroencephalogram (EEG)

Communication at neuron level within the brain is an electrochemical process. Action potential at the synaptic cleft triggers release of neurotransmitters which eventually causes postsynaptic potentials. These post-synaptic potentials produce a current flow, also called current dipole, lasting for around tens to hundreds of milliseconds (Kirschstein & Köhling, 2009). In the event of a regional activation, millions of post-synaptic potentials occur together (Nunez & Srinivasan, 2006). The EEG is a physiological recording device used to detect these current dipoles through electrodes located on the human scalp (Berger, 1929).

Due to its non-invasive nature and low cost, the EEG has become widely used in many clinical and research applications. Moreover, its high temporal resolution makes EEG a preferred method of choice for fast cognitive processes (Gomez-Herrero, 2010).

Magnetoencephalogram (MEG)

Current flow produced by postsynaptic potentials also produce a magnetic field which can be measured from outside the skull (Feynman, Leighton, & Sands, 1964; Cohen D. , 1968). Magnetoencephalogram (MEG) is a physiological recording device measuring this magnetic field through magnetometers (Hämäläinen, Hari, Ilmoniemi, Knuutila, & Lounasmaa, 1993). However, the strength of brain's magnetic field is as low as 50-500 fT (Hämäläinen, Hari, Ilmoniemi, Knuutila, & Lounasmaa, 1993), making it very difficult to detect in comparison to ambient magnetic fields. Figure 2.7 shows a scale for surrounding magnetic fields (Tanzer, 2006). In order to alleviate this problem, state of the art MEG devices use superconducting quantum interference device (SQUID) magnetometers and data acquisition takes place in heavily shielded rooms (Zimmerman, Thiene, & Harding, 1970; Cohen D. , 1970).
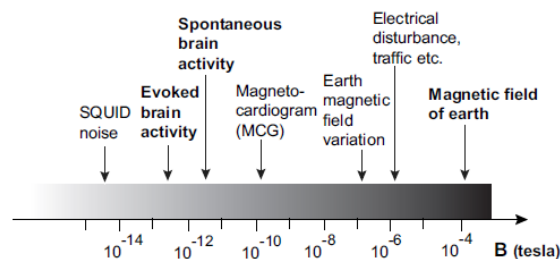
Figure 2.7: Magnetic Field Strengths. The magnetic field of brain activity is very low compared to surrounding magnetic fields. Thus, SQUID magnetometers and heavily shielded rooms are used[7].

Due to properties of the magnetic field, radial dipoles are invisible to MEG (Ahlfors, Han, Belliveau, & Hämäläinen, 2010) while EEG detects both radial and tangential dipoles (Figure 2.8). Even though MEG detects only the tangential dipoles, its spatial resolution in separating cortical sources is proven to be better than EEG, making it a reason for preference (Hari, 2011).

Among non-invasive neuroimaging techniques, EEG and MEG systems have the highest temporal resolution (milliseconds) available (Hämäläinen, Hari, Ilmoniemi, Knuutila, & Lounasmaa, 1993). There are studies combining MEG and EEG to increase spatiotemporal resolution (Sharon, Hämäläinen, Tootell, Halgren, & Belliveau, 2007).

---

[7] Figure from (Tanzer, 2006)
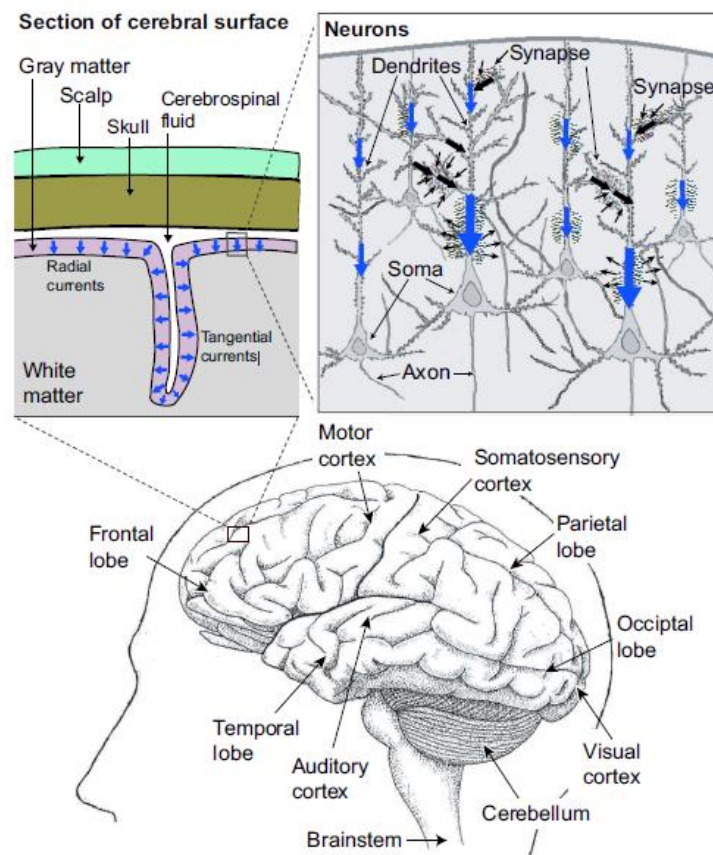
Figure 2.8: Organization of Neurons. Pyramidal neurons are oriented normal to the cortex surface. MEG is insensitive to radial dipoles[8].

2.2.2 Source Localization

Technological developments in the past several decades offer the potential for E/MEG to produce accurate estimates of the location and time courses of brain activity (Mosher, Leahy, & Lewis, 1999). There are two important concepts of source localization; *forward solution* and *inverse problem*. The forward solution is the estimation of the signals to be measured on the scalp due to a dipole activity in a specific brain region (Cohen M. X., 2014). On the other hand, the inverse problem is the estimation of source activity with exact location and amplitude based on the measured signals on the scalp (Cohen M. X., 2014).

Forward Problem

In order to calculate forward solution, head as a volume conductor and the underlying neural sources should be modeled (Baillet S. , Forward and Inverse Problems of

---

[8] Figure adapted from (Hämäläinen, Hari, Ilmoniemi, Knuutila, & Lounasmaa, 1993)

11

MEG/EEG, 2014). Several different approaches exist in the context of head modeling. The earliest analytic models assumed the head as an isotropic sphere while more realistic versions included a set of nested spheres representing scalp, skull layers, gray matter and white matter with different conductivity properties (Sarvas, 1987; Huang, Mosher, & Leahy, 1999). Although head models with spherical approaches are easy to model, they are not accurate as the human brain is not spherical (Stenroos & Sarvas, 2012). Latest approaches including Boundary Element Model (BEM) and Finite Element Model (FEM) provide more realistic approximations (Ramírez, 2008). Both approaches require extracting anatomical information from the subject's MRI or using a template MRI. BEM uses homogeneous and isotropic conduction properties within each tissue layer while FEM allows modeling anisotropy within same tissue layers (Marin, Guérin, Baillet, Meunier, & Meunier, 1998). Because of complication and difficulty of modeling with FEM, BEM models are used widely in the field (Baillet, Friston, & Oostenveld, 2011). The output of the forward solution is a weight matrix called Lead-Field, which is used in inverse solution algorithms.

Inverse Problem

The inverse problem is an ill-posed problem due to an infinite number of solutions. In order to calculate an inverse solution, prior assumptions should be made (Baillet, Mosher, & Leahy, 2001). There are three basic approaches for inverse solutions (Ramírez, 2008):

I. *Parametric Dipole Modelling:* Dipole modeling assumes that the measured signals were generated by few regions in the brain. These regions are modeled as Equivalent Current Dipoles (ECD) Bayesian particle filtering methods are found useful for the solution (Solin, et al., 2016). Lately, these approaches are abandoned in the favor of relatively newer methods (Baillet S. , 2014).

II. *Beamforming:* Beamforming methods are based on radar data analysis methods. A set of dipoles are defined in the brain and each dipole is evaluated separately in means of data fitting while ignoring the information content of other dipoles (Baillet S. , 2014). Beamforming methods are well studied and frequently used in the field. Multiple Signal Classification (MUSIC) (Schmidt, 1986), Linearly Constrained Minimum-Variance Beamforming (LCMV) (Van Veen, van Drongelen, Yuchtman, & Suzuki, 1997), Synthetic Aperture Magnetometry (SAM) (Robinson & Vrba, 1999), and Dynamic Imaging of Coherent Sources (DICS) (Gross, et al., 2001) are few of the most known beamforming algorithms. In this study, LCMV algorithm is used for source localization.

III. *Distributed Source Imaging*: Distributed source imaging assigns dipoles at every possible candidate location, making the inverse solution heavily underdetermined. Prior information is provided in order to solve the inverse problem. Although distributed source imaging is computationally expensive, lately new algorithms are introduced (Solin, et al., 2016). In general, most

popular algorithms are weighted minimum-norm image models (Baillet S. , 2014).

Volume Conduction Problem

Volume conduction problem, also known as field spread, is caused by the interaction of multiple channels with a single source (Brookes, et al., 2011). This interaction creates a major problem with MEG/EEG source estimation. Source estimates are spatially correlated and the leakage of source activity due to shared sensors result in fake active regions in the neighborhood of genuinely active neurons (Palva & Palva, 2012). Even though source estimation methods such as Dynamic Imaging of Coherent Sources (DICS) and Linearly Constrained Minimum Variance Scalar Beamformer (LCMV) show limited susceptibility to volume conduction problem, effects still cannot be totally eliminated (Drakesmith, El-Deredy, & Welbourne, 2013; Schoffelen & Gross, 2009). Thus, it is also important to use connectivity measures which are prone to volume conduction.

2.2.3 Functional Connectivity Analysis

Bivariate interactions in the brain can be investigated in two different types: linear interactions and nonlinear interactions (Sakkalis, 2011).

Linear Interactions

Investigation of linear interactions assumes that the interactions are products of linear systems. In a linear system, scaling the input by a factor gets the output scaled by the same factor (Hansen, Kringelbach, & Salmelin, 2010). Linear measures are well investigated in the brain at various task related and resting state data. Cross-correlation, coherence and imaginary coherency are mostly used linear measures. Within the scope of this study, Coherence and Imaginary Coherency measures are used to evaluate linear interactions.

Coherence

Coherence is defined as the normalized version of cross-spectrum; Fourier transform of the cross-correlation (David, Cosmelli, & Friston, 2003). Coherence takes values between 0 and 1, with 0 meaning that there is no correlation between signals and 1 meaning that the signals are proportional. Coherence is sensitive to both power and the phase of two signals (Sakkalis, 2011). Earlier studies showed that Coherence is a useful measure for detecting long-range interactions (Gross, et al., 2001; Nunezab, et al., 1997).

Imaginary Coherency

Due to volume conduction effect, a single activity of a dipole is observable in more than one channels outside the head (Sarvas, 1987), showing an artifact rather than true interaction (Nolte, et al., 2004). In order to avoid volume conduction effect, Nolte et

al. developed Imaginary Coherency with the idea that scalp potential has no time-lag to underlying source activity (Stinstra & Peters, 1988). The imaginary part of coherency is blind to synchronizations with no time-lag, making it blind to artefactual self-interaction caused by volume conduction also (Nolte, et al., 2004). Robustness of Imaginary Coherency to volume conduction effect was later verified by following studies and popularity of the measure has increased (Sander, Bock, Leistner, Kühn, & Trahms, 2010; Domínguez, Stieben, Pérez Velázquez, & Shanker, 2013; Hohlefeld, et al., 2013).

Nonlinear Interactions

The nervous system is considered as a nonlinear, dynamical system (Aydore, Pantazis, & Leahy, 2013; Stam, Breakspear, van Walsum, & van Dijk, 2003). Nonlinear relations between spatially distant regions have been shown to be important (Breakspear & Terry, 2002). Various phase estimation and cross-frequency measures are used frequently to investigate functional connectivity caused by nonlinear systems (Jirsa & Müller, 2013; Özkurt & Schnitzler, 2011; Florin & Baillet, 2015; Colclough, et al., 2016).

Quadratic Phase Coupling

An important class of cross-frequency coupling, Quadratic Phase Coupling, has gained attention lately. QPC originates as a result of a nonlinear system in the brain and it is expressed as (Isler, Grieve, Czernochowski, Stark, & Friedman, 2008);

$$2\pi f_3 t + \varphi_3 = (2\pi f_1 t + \varphi_1) + (2\pi f_2 t + \varphi_2) \qquad (2.1)$$

requiring both $f_3 = f_1 + f_2$ and $\varphi_3 = \varphi_1 + \varphi_2$ (Venkatakrishnan, Sukanesh, & Sangeetha, 2011).

Bispectrum

In general, bispectrum is a statistical measure used to search for nonlinear interactions. Bispectrum is evaluated in the category of higher-order spectra and it provides supplementary information to the power spectrum. Higher order spectral measures are extensions to second-order measures known as autocorrelation. Bispectrum is the Fourier Transform of the third-order cumulant sequence just as power spectrum is the Fourier Transform of second order (Nikias & Mendel, 1993). The bispectrum of three zero-mean third order stationary random processes *x,y* and *z* is given below:

$$B_{xyz}(\omega_1, \omega_2) = \Sigma_{m=-\infty}^{\infty} \Sigma_{n=-\infty}^{\infty} R_{xyz}(m,n) e^{-j(m\omega_1 + n\omega_2)} \qquad (2.2)$$

$$R_{xyz}(m,n) = E\{x(k)y(k+m)z(k+n)\} \qquad (2.3)$$

where ω represents angular frequency, *m* and *n* independent lags, *E{}* expectation operator and R_{xyz} third-order cumulant.

Bicoherence

Bicoherence the normalized version of bispectrum and it is a powerful tool to detect QPC types of nonlinear interactions. It has been applied successfully to evaluate nonlinear effects in human EEG and MEG (Barnett, Johnson, Naitoh, Hicks, & Nute, 1971; Dumermuth, Huber, Kleiner, & Gasser, 1971; Nikias & Mendel, 1993). Although proven useful in many signal processing fields, bicoherence has not been used widely in neuroscience due to computational costs (Özkurt T. E., 2016) and volume conduction effect (Pereda, Quiroga, & Bhattacharya, 2005).

In order to reduce computational costs, researchers suggested new methods. Sensor level PCA was applied by Chella et al. (2014) to reduce the data dimension. This approach actually only lowers the computational cost if only the sensor level bicoherence is considered. It is not applicable to source level bicoherence computation. On the other hand, Özkurt (2016) suggested using 'sliced bicoherence' to reduce the computational costs with the idea that the most prominent interactions are located on the main diagonal of the bicoherence matrix. Sliced bicoherence is an indirect method only calculating the main diagonal of the bicoherence matrix.

In order to alleviate volume conduction problem, (Chella, Marzetti, Pizzella, Zappasodi, & Nolte, 2014) suggested removing the antisymmetric part of the bicoherence to eliminate 'autobispectra' of sources. On the other hand, (Özkurt T. E., 2016), suggests another method which also eliminates channel related 'autobispectra' as well. Suggested method, called 'subtracted bicoherence' only keeps the 'cross' relations between sources.

CHAPTER 3

MATERIALS AND METHODS

3.1 Materials

MEG Data

Publicly available resting-state MEG recordings collected in the scope of HCP were used in this study (Van Essen, et al., 2013). MEG recordings are part of S1200 release and details of the scanning procedures are provided by the S1200 Release Reference Manual (WU-Minn HCP Consortium, 2017). The data consist of 89 MEG subjects and all subjects are young adults (ages 22-25) with a subset of ~50 same-sex twin pairs.

All subjects were scanned with a whole head Magnes 3600 Scanner (4D Neuroimaging, San Diego, CA, USA) in a magnetically shielded room. Subjects were also scanned with 3T MRI (Siemens 3T "Connectome Skyra", St. Louis, MO, USA) scanner in order to acquire anatomical information. Magnes 3600 system includes 248 magnetometer channels together with 23 reference channels. Data were sampled at 2034.5101 Hz. In order to remove cardiac and ocular activity, electrooculography (EOG, 2 channels) and electrocardiography (ECG, 1 channel) recordings were synchronized with the MEG. Participants were positioned supine in the MEG scanner. In order to co-register MEG data to the MRI scans, a 3-point reference system (nasion and two peri-auricular points) and locator coils were used.

Resting state MEG data were recorded in 3 consecutive sessions for each subject for approximately 6 min. We selected one of three sessions randomly for this study. The data provided by HCP were preprocessed, resampled at 508.625 Hz. and saved in Fieldtrip file format. Bad channels, bad segments and remaining artifacts were removed using ICA. Cardiac components and eye-blinks were also cleaned from the data in this scope.

Software and Auxiliary Toolboxes

All computations in this thesis were implemented in MATLAB® (R2017a, The Mathworks Inc., Natick, MA). Publicly available Fieldtrip Toolbox (Oostenveld, Fries, Maris, & Schoffelen, 2011), Higher Order Spectral Analysis (HOSA) (Swami, Mendel, & Nikias, 1993) Toolbox and MEG Connectome Pipelines (WU-Minn HCP Consortium, 2017) were used for some of the calculations.

Parcellation Atlas

In order to reduce the data dimension, identify Anatomical Volumes of Interest (AVOI) and create group level results, Automated Anatomical Labelling (AAL) Atlas

was used (Tzourio-Mazoyer, Landeau, Papathanassiou, Crivello, & Etard, 2002). Original AAL Atlas includes 45 AVOIs in each hemisphere with a total of 90 AVOIs. AAL Atlas used in this study is based on the original atlas with the addition of cerebellum and vermis reaching a total number of 116 AVOIs (Neurofunctional Imaging Group-GIN, UMR6232, CYCERON, Caen, France). Table 1 and Figure 3.1 provide detailed information about the atlas used in this study.

Table 1: Anatomical Volumes of Interest. AAL 90 Atlas, made available by Neurofunctional Imaging Group (Caen, France), was used. The Atlas used in this study is based on the original atlas developed by Tzourio-Mazoyer which contains 45 AVOI in each hemisphere excluding Cerebellum and Vermis (Tzourio-Mazoyer, Landeau, Papathanassiou, Crivello, & Etard, 2002). Given volume of each AVOI in the table is the ratio of the total volume of the AVOI in both hemispheres to total volume of the brain. Given distance is the distance of the center of gravity of each AVOI to the closest magnetometer.

ROI	Anatomical ROI	Vol. (%)	Dist. (mm)	ROI	Anatomical ROI	Vol. (%)	Dist. (mm)
1	Precentral	2,68	42,04	25	Occipital_Sup	1,44	55,47
2	Frontal_Sup	2,47	55,82	26	Occipital_Mid	2,81	53,52
3	Frontal_Sup_Orb	0,34	68,37	27	Occipital_Inf	1,10	53,72
4	Frontal_Mid	4,32	51,46	28	Fusiform	2,40	75,03
5	Frontal_Mid_Orb	0,96	56,46	29	Postcentral	3,16	43,99
6	Frontal_Inf_Oper	1,37	48,21	30	Parietal_Sup	0,96	42,77
7	Frontal_Inf_Tri	2,33	49,36	31	Parietal_Inf	1,78	44,19
8	Frontal_Inf_Orb	1,92	56,31	32	SupraMarginal	1,78	44,81
9	Rolandic_Oper	1,10	53,01	33	Angular	1,65	48,21
10	Supp_Motor_Area	1,65	48,84	34	Precuneus	3,09	60,04
11	Olfactory	0,27	87,89	35	Paracentral_Lobule	0,55	39,30
12	Frontal_Sup_Medial	3,23	54,19	36	Caudate	0,62	83,09
13	Frontal_Med_Orb	1,17	69,69	37	Putamen	0,96	72,20
14	Rectus	0,69	85,30	38	Pallidum	0,21	85,70
15	Insula	1,51	61,22	39	Thalamus	1,10	86,07
16	Cingulum_Ant	1,37	70,46	40	Heschl	0,27	72,59
17	Cingulum_Mid	2,68	63,78	41	Temporal_Sup	2,81	51,12
18	Cingulum_Post	0,41	83,16	42	Temporal_Pole_Sup	1,37	54,92
19	Hippocampus	0,89	78,33	43	Temporal_Mid	4,80	53,82
20	ParaHippocampal	0,89	83,03	44	Temporal_Pole_Mid	1,24	57,28
21	Amygdala	0,21	82,63	45	Temporal_Inf	2,61	58,14
22	Calcarine	2,40	68,94	46	Cerebellum	7,69	58,66
23	Cuneus	1,65	58,86	47	Vermis	1,03	62,03
24	Lingual	2,06	75,87				
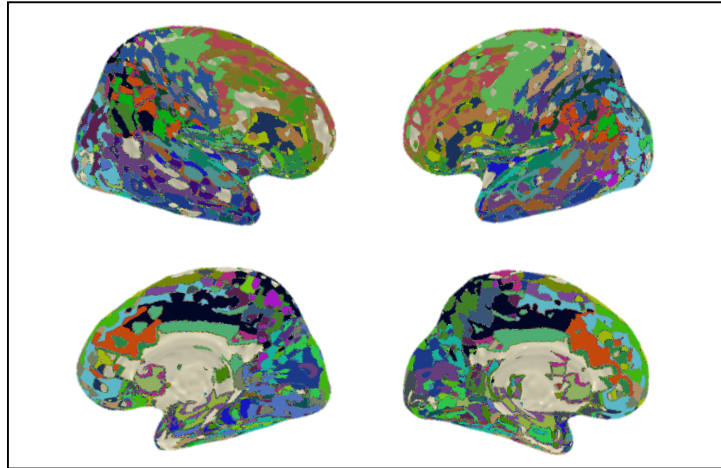
Figure 3.1: Representation of AAL Atlas. Different colors are used for seperate AVOIs.

3.2   Data Processing

The workflow followed in the scope of this thesis is given at Figure 3.2. The rest of this chapter will describe given steps in detail.

Import Data
Resting State Data,
Anatomical Information

Source Localization
Boundary Element Model
LCMV Beamformer

Dimension Reduction
Principal Component
Analysis (PCA)

Bicoherence Analysis
Higher Order Spectral
Analysis Toolbox

Statistical Analysis
Diagonal Components
Non-Diagonal Components

Linear/Nonlinear Estimation
Sliced/Subtracted Bicoherence
Coherence/Imaginary Coherency

Statistical Analysis
Reliability Analysis
Correlation Analysis

Figure 3.2: Workflow of the Study. Details are described in further detail in this chapter.

3.2.1 Forward Solution

In order to calculate forward solution, a volume conductor and a neural source model should be modeled (Baillet S. , 2014). Volume conduction model used in this study is the subject specific headmodel provided by HCP. A neural source model for each subject was created with a 10 mm grid using subject specific MRI. As a result, a neural source model of~1500 voxels was created for each subject. Figure 3.3 shows a headmodel and a sourcemodel for an exemplary subject.

Using created sourcemodel, subject specific headmodel, sensor locations and sensor readings from resting state data, a leadfield matrix was calculated. Leadfield matrix represents an *M*3* weight matrix at each voxel, where *M* denotes the number of channels. Weight matrix includes information for 3 dipole orientations *(-x,-y,-z)*.
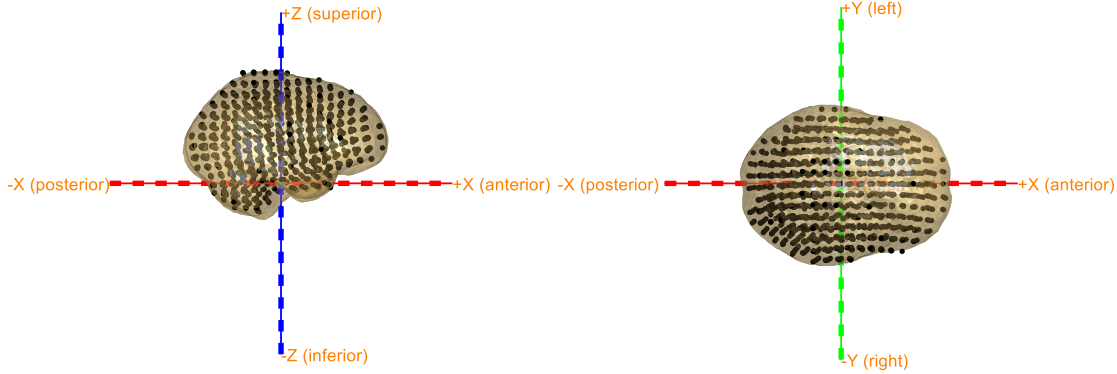
Figure 3.3: Sourcemodel and Headmodel Representations. Sourcemodel is located inside a headmodel with sagittal and axial views. Representative subject from HCP Data.

3.2.2 Inverse Solution

Source construction was realized using LCMV (Van Veen, van Drongelen, Yuchtman, & Suzuki, 1997). Leadfield matrix was reduced 1 dipole orientation with most variance for each voxel using Single Value Decomposition. Calculation of LCMV Beamformer is given below;

$$A_S = W_S^T B \qquad\qquad (3.1)$$

$$W_S^T = (L_S^T C^{-1} L_S)^{-1} L_S^T C^{-1} \qquad\qquad (3.2)$$

Where A_S is the source level data, W_S is the spatial filter, B is the sensor level data, L_S is the leadfield matrix, and C is the covariance matrix.

3.2.3 Group Level Analysis and Dimension Reduction

In order to make group level analysis over 89 subjects, AAL Atlas was used. Source level data of each subject were sorted out according to AVOI information and PCA was applied to reduce grouped time-series to representative signals. Results of each AVOI over 89 subjects were projected to a template brain provided by Fieldtrip (Oostenveld, Fries, Maris, & Schoffelen, 2011).

Aforementioned PCA reduction was carried out in a way that each region preserved 90% of its information. Depending on the information content of the region, some regions preserved more than one time-series. The number of virtual time-series is subject specific, ranging from 210 to 280 with the average of ~250. Figure 3.4 shows an exemplary PCA reduction.
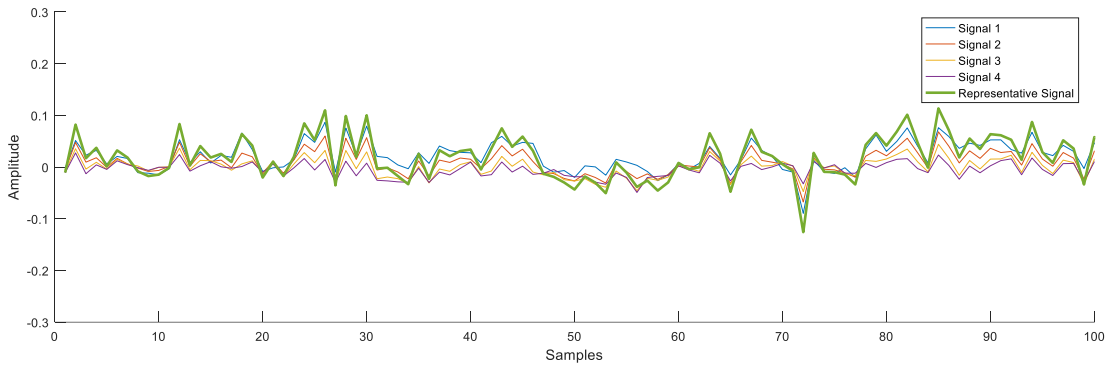
Figure 3.4: Dimension Reduction Using PCA. An exemplary AVOI is shown for visualization. PCA was used to reduce four source-space signals in an AVOI to a single representative signal.

3.2.4 Bicoherence Estimation

HOSA Toolbox (Swami, Mendel, & Nikias, 1993) was used for Bicoherence estimation in this study. For each subject, Bicoherence Matrix was calculated $N*N$ times where N is the number of virtual time series. The data was segmented into non-overlapping 256 sample hanning windows. Windowing of the data leads to a 4 Hz of spectral resolution limit. The mean was removed from each record and the Fast Fourier Transform was computed. Calculation of Cross Bicoherence between time-series $x(t)$ and $y(t)$ is given as below;

$$b_{ij} = \frac{|E\{X(f_1)X(f_2)Y^*(f_1 + f_2)\}|^2}{S_X(f_1)S_X(f_2)S_Y(f_1 + f_2)} \tag{3.3}$$

where superscript * denotes complex conjugate and E{ } is the statistical expectation operator (Elgar, Van Atta, & Gharib, 1990). Here, *X* and *S* denote Fourier coefficients and spectra, respectively.

21

Confidence Level Calculation

An empirical confidence level for each subject was calculated using Bootstrapping Resampling Method (Efron, 1979). Randomly chosen 5 virtual time-series pairs were used for calculation. For each pair, one of the signals was divided into 256 sample pieces and shuffled 100 times to calculate bicoherence repeatedly. As a result, 500 different bicoherence matrices were produced for each subject. At each frequency pair, the 95% limit of the distribution was assigned as the confidence level. Confidence Level was used for each subject to threshold the bicoherence results separately.

Thresholding and Evaluation

Each bicoherence matrix was thresholded using subject specific confidence level. Values of frequency pairs above confidence level were accepted significant and represented with '1'. The remaining values were assigned '0', making a binary matrix. Entire sets of bicoherence matrices calculated for each subject were used to calculate the percentage of significant bicoherence of each frequency pair.

3.2.5 Coherence and Imaginary Coherency Calculation

Coherence calculation within the scope of this study was 'Magnitude-Squared Coherence Estimate'. Coherency with the given formula below was calculated for each pair of the time-series;

$$C_{ij} = \frac{E\{X_i(f)X_j^*(f)\}}{(S_i(f)S_j(f))^{1/2}} \qquad (3.4)$$

where superscript * denotes complex conjugate and E{} is the statistical expectation operator. Coherence and Imaginary Coherency were calculated with below formulas;

$$Coh_{ij}(f) = |C_{ij}|^2 \qquad (3.5)$$

$$Im.\ Coh_{ij}(f) = |Im(C_{ij})|^2 \qquad (3.6)$$

where C_{ij} is the Coherency (Eq. 3.4) and Im() denotes the imaginary part. Coherence and imaginary coherency results are represented in AVOI matrices. In order to achieve this, coherence and imaginary coherency were calculated for each possible pair in each opposing AVOI. Maximum connectivity result for each AVOI is used in the final matrix.

3.2.6 Sliced and Subtracted Bicoherence Calculation

Sliced and subtracted bicoherence calculation routines used in this study were developed by Özkurt (2016). Sliced bicoherence metric uses an indirect formula to compute cross-bispectral slice:

$$b_{112}(f, f) = \mathcal{F}\{x_1(n) * x_1(n) * y_2(n)\} \qquad (3.7)$$

where $\mathcal{F}$ stands for Discrete Fourier Transform, $*$ is the convolution operator and

$$y_2(n) = \begin{cases} x_2(N - 1 - n/2), & n \text{ is even} \\ 0, & n \text{ is odd} \end{cases} \qquad (3.8)$$

On the other hand, Subtracted Bicoherence is an alternative metric of Sliced Bicoherence being robust to volume conduction (Özkurt T. E., 2016). Subtracted bicoherence eliminates strong autobispectral relations and only conserves "cross" connectivity between channels. Subtracted bicoherence formulation is given as below:

$$\widetilde{b_{12}}(f) = \begin{cases} b_{12}(f) - b_{11}(f), & if\ b_{12}(f) - b_{11}(f) > 0 \\ 0, & if\ b_{12}(f) - b_{11}(f) \le 0 \end{cases} \qquad (3.9)$$

3.2.7 Statistical Comparison

The metrics described here were also compared with each other in means of both correlation and reliability.

Correlation

We used Pearson's correlation to investigate similarities between metrics. Correlation analyses were carried out for each AVOI. We compared Coherence with Sliced Bicoherence and Imaginary Coherency with Subtracted Bicoherence. Percentage of significantly ($p<0.05$) correlated AVOIs to total number of AVOIs was calculated for each correlation analysis.

Split Half Reliability Test

Reliability of each measure was calculated using Split Half Reliability Test (Colclough, et al., 2016). Subjects were divided to half 100 times and average scores of 2 sets for each AVOI was calculated and compared every time.

3.2.8 Computational Cost

The high computational cost of bicoherence estimation arises from the high number of calculations. A pairwise bicoherence analysis of multivariate source data requires estimates in the order of $N^2 x\ (M^2/2)$, where N and M denote the number of channels/sources and the number of sampled frequencies, respectively. Number of estimated sources in our study is ~1500 per each subject. After PCA reduction, the number of sources is reduced to ~250.

The bicoherence is symmetric under the transformations *(ω1,ω2) → (ω2,ω1)* and *(ω1,ω2) → (-ω1,-ω2)*, so that only one quarter of the plane *(ω1,ω2)* contains independent information. Considering that the sampling frequency for resting state MEG data, total number of meaningful frequency bins is ~128.

Total bicoherence estimation calculates bicoherence at each frequency bin and in our study the number of calculations equals to ~512.000.000 ($250^2 \times (128^2/2)$) per each windowed segment for every subject. 5-min MEG recording with 508.625 Hz sampling frequency is windowed with 256 sample hanning window, creating ~600 segments. As a result, the total number of calculations reaches over 300.000.000.000 per subject. Total bicoherence estimation per a subject takes ~50 hours on an above average computer. Total calculations for this thesis took almost 2 months with 4 different computers working simultaneously.

Sliced and subtracted bicoherence only calculate the main diagonal which consists of a total of 128 frequency bins($f_1 = f_2$). The reduction of the number of frequency bins reduces the number of calculations drastically. As a result, calculation time is reduced to 1/60 of total bicoherence estimation.

CHAPTER 4

RESULTS

The 'Results' section of the study is divided into two sections. First section concentrates on total Bicoherence Matrix, evaluates cross frequency interactions and identifies information content of the matrix. Second section compares linear and nonlinear connectivity analysis methods.

4.1   Total Bicoherence Matrix

Total Bicoherence Matrix represents information content of each frequency pair (128x128). As explained in Chapter 3.2.4, value of each frequency pair represents percentage of that pair showing significant bicoherence.

Total Bicoherence Matrix shows that there are several important interactions within and cross frequency bands. As expected at resting state data, the most prominent interaction is visual at the alpha band (8-12 Hz.) (Figure 4.1). Even though the interaction points to $f_1 = f_2$, it is interpreted as $f_2 = 2f_1$ interaction due to bicoherence formulation (3.3). As a result, the interaction at alpha band points to a true interaction between alpha and beta bands. Similar fashion could be observed at delta and theta bands pointing to delta-theta, delta-alpha, theta-alpha and theta-beta interactions. It is quite difficult to analyze interactions below alpha band separately because of the frequency resolution used for this study (4 Hz). It is clearly seen that most of the nonlinear interaction between brain regions mainly concentrates at the main diagonal of the bicoherence matrix pointing to $f_2 = 2f_1$ interactions.

As explained earlier, in order to find Total Bicoherence Matrix, subject specific confidence level matrices were calculated empirically.

Figure 4.2 shows one-sided Confidence Level Matrix averaged across 89 subjects. The empirically found confidence level confirms earlier works on parametric confidence level calculation used by Özkurt (2016) with an important note on the diagonal components. Özkurt (2016) suggested that the confidence level for the components at the main diagonal is twice the confidence level at the non-diagonal components. Our empirical calculations show that this depends on the frequency resolution of the calculations. The confidence level tends to increase as the component approaches the main diagonal and maximizes at the main diagonal, reaching double the confidence level of non-diagonal components. We sliced the confidence level matrix beginning from the main diagonal to the left bottom of the matrix and calculated the average of each slice. The reduced confidence level graph is shown at Figure 4.3. The confidence level decreases as the distance between the slice and the main diagonal increases. It is important to note that the first 4 slices have higher confidence level compared to other slices. This corresponds to 4 Hz. Frequency resolution used in the study. Taking the

frequency resolution into consideration, first 4 slices are identified as the diagonal components since they are effected by the frequency leakage.

We investigated the information content of the bicoherence matrix and compared diagonal components to non-diagonal components. Figure 4.4 shows mean and standard error graph for Total Bicoherence Matrix for all of the subjects. The figure shows clear separation between diagonal and non-diagonal components in means of information content for each subject. We also investigated the information content of each AVOI and found the same pattern (Figure 4.5). Moreover, we applied t-test for both subject level and region level comparisons and found significant separation ($p<0.05$) between diagonal and nondiagonal components. Both figures show that the information content of the bicoherence matrix is mostly concentrated on the diagonal components, pointing to 2nd order couplings of the resting state brain at $f_2 = 2f_1$.
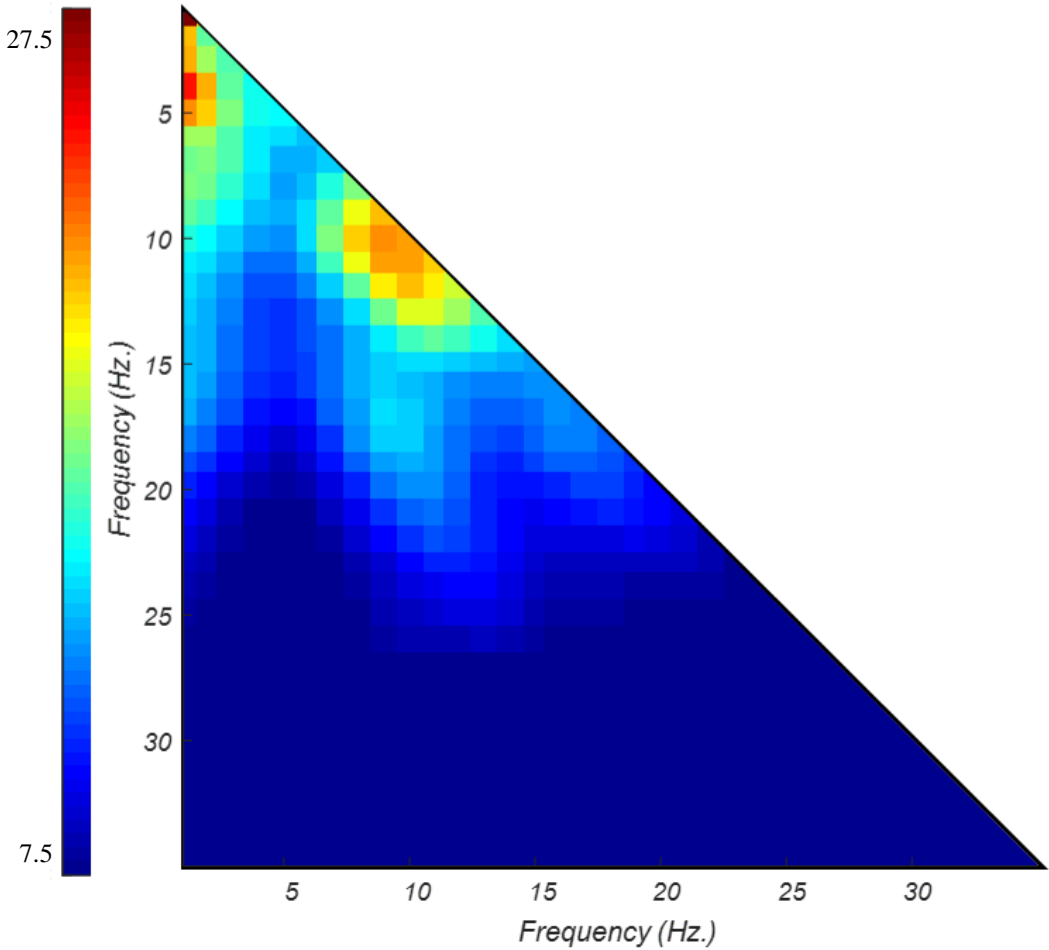

Figure 4.1: Total Bicoherence Results. Mean Bicoherence Matrices calculated over 89 subjects. Color Bar indicates percentage of each frequency pair showing significant bicoherence at corresponding frequencies. Note the interactions at Alpha Band (8-12 Hz).

26
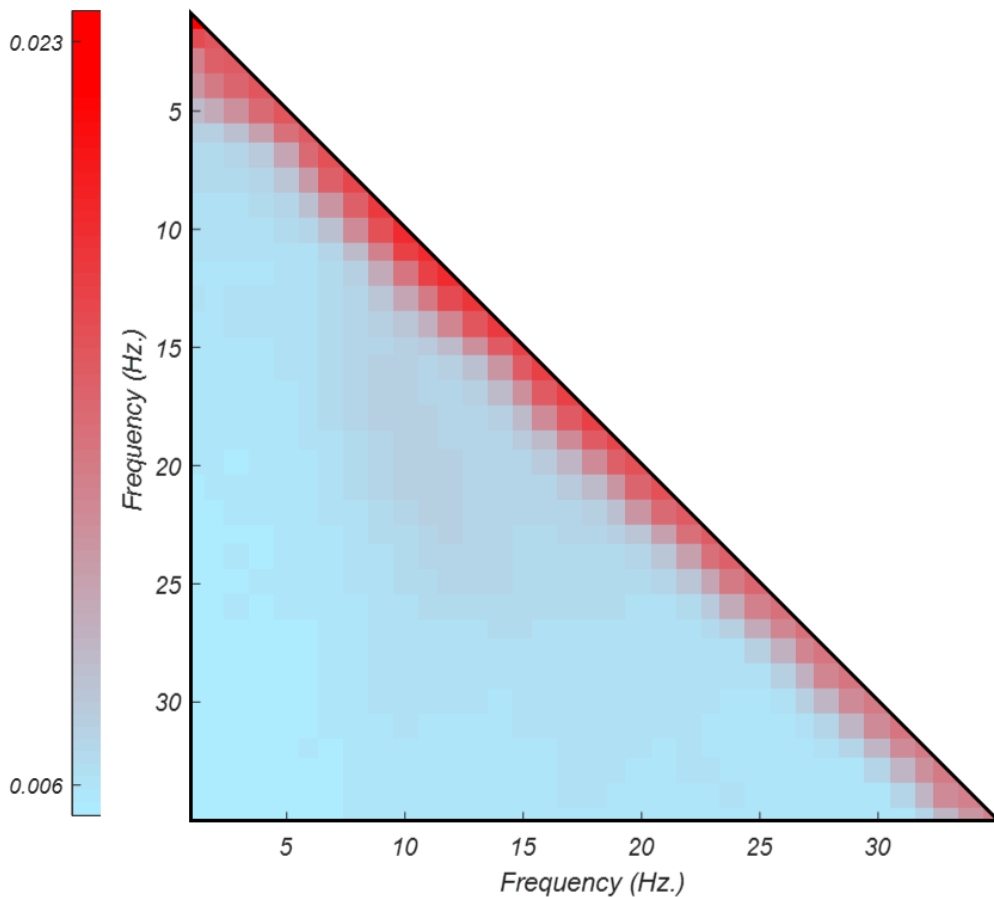
Figure 4.2: Empirically Calculated %95 Confidence Level Matrix. Color Bar indicates confidence level averaged across subjects. Confidence level increases as the components approach the main diagonal, reaching double the confidence level of non-diagonal components.
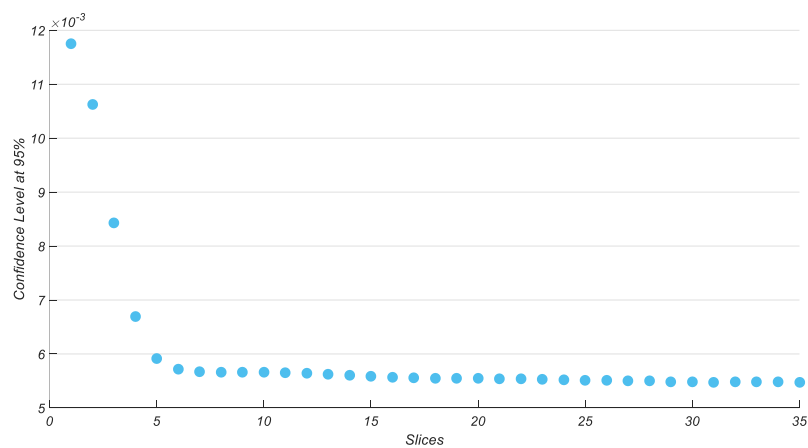
Figure 4.3: Reduced Confidence Level. First 4 slices belonging to the main diagonal show higher confidence levels due to 4 Hz. frequency resolution. The nondiagonal slices show half the confidence level when compared to the diagonal slices. These results confirm parametric confidence level calculation method.
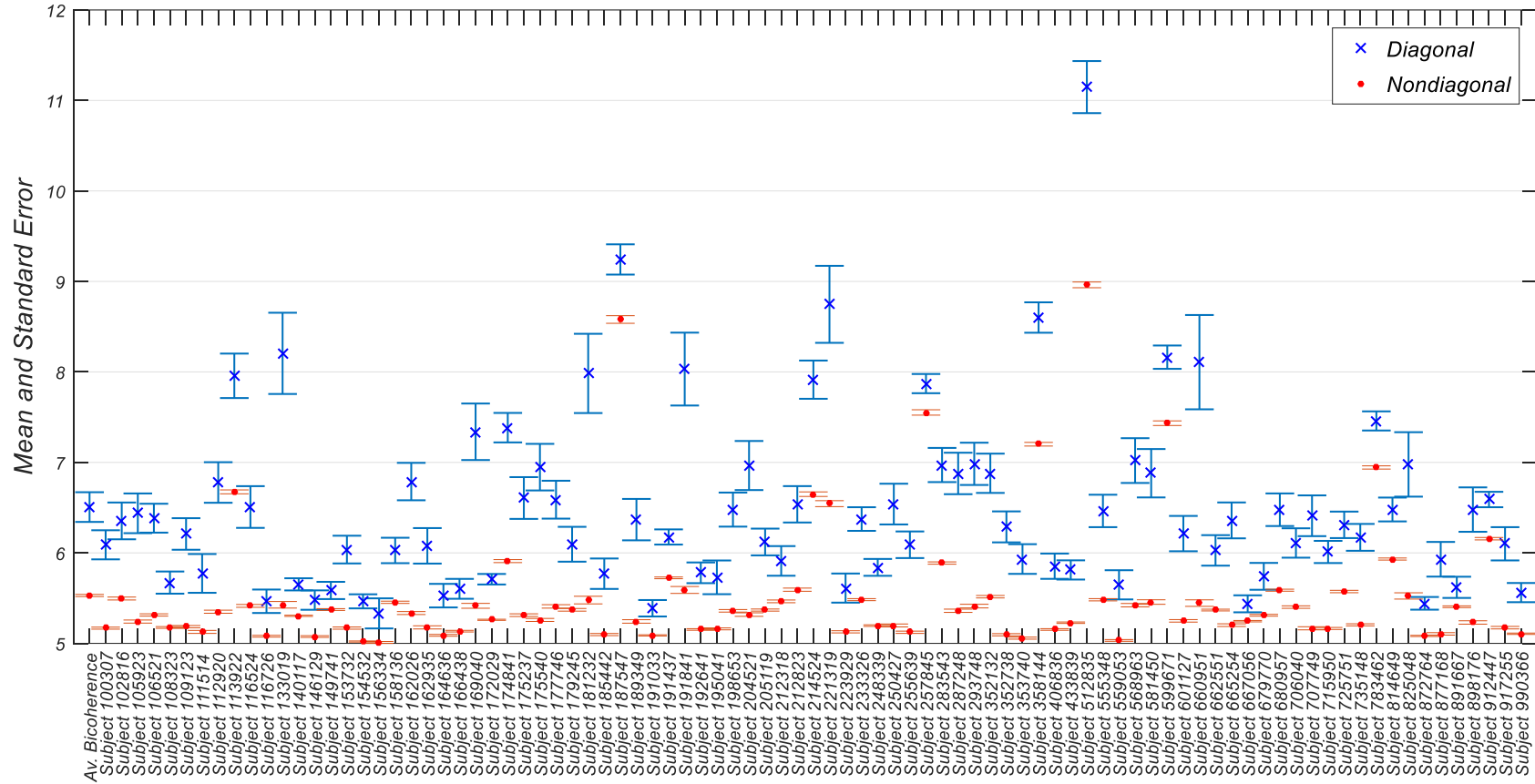
Figure 4.4: Mean and Standard Error of Diagonal and Non-Diagonal Components. First 4 diagonals were marked as Diagonal Components due to frequency resolution. Mean and Standard Error indicates percentage of cross coupling at either diagonal frequencies or non-diagonal frequencies. Figure shows clear separation for both average and individual bicoherence matrices, indicating high information content of diagonal components.
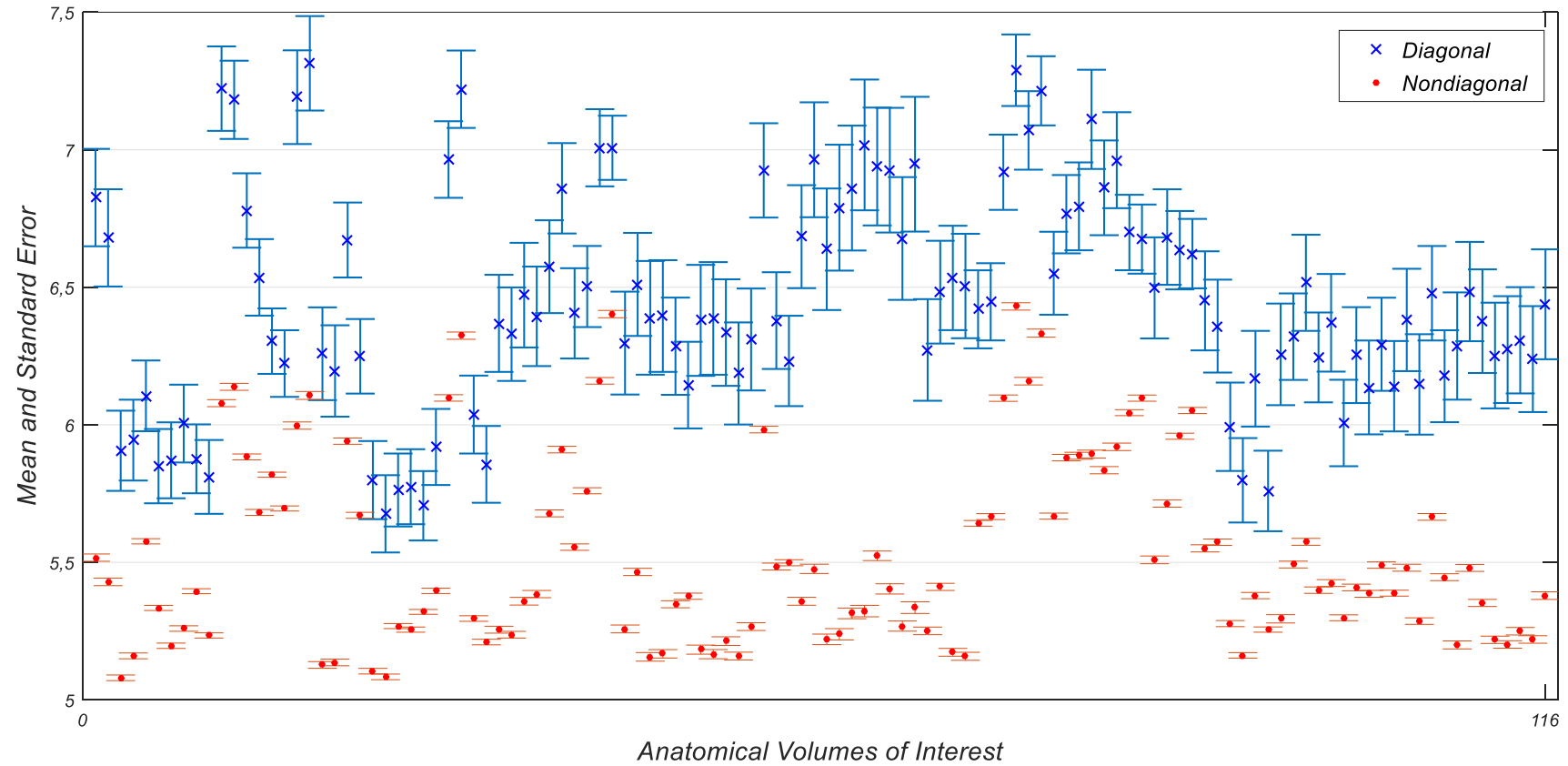
Figure 4.5: Diagonal and Non-Diagonal components of AVOIs. First 4 diagonals were marked as Diagonal Components due to frequency resolution. Mean and Standard Error indicates percentage of cross coupling at either diagonal frequencies or non-diagonal frequencies. Clear separation of information content at each AVOI follows the same pattern of total bicoherence matrix.

4.2   Comparison Between Linear and Nonlinear Couplings

As our findings suggest that the prominent nonlinear interactions are concentrated on the diagonal components, we compared two main diagonal based nonlinear methods to linear methods. Linear interaction analyses were carried out using coherence and imaginary coherency metrics. On the other hand, nonlinear interaction analysis were carried out using Sliced Bicoherence and Subtracted Bicoherence metrics suggested by Özkurt (2016).
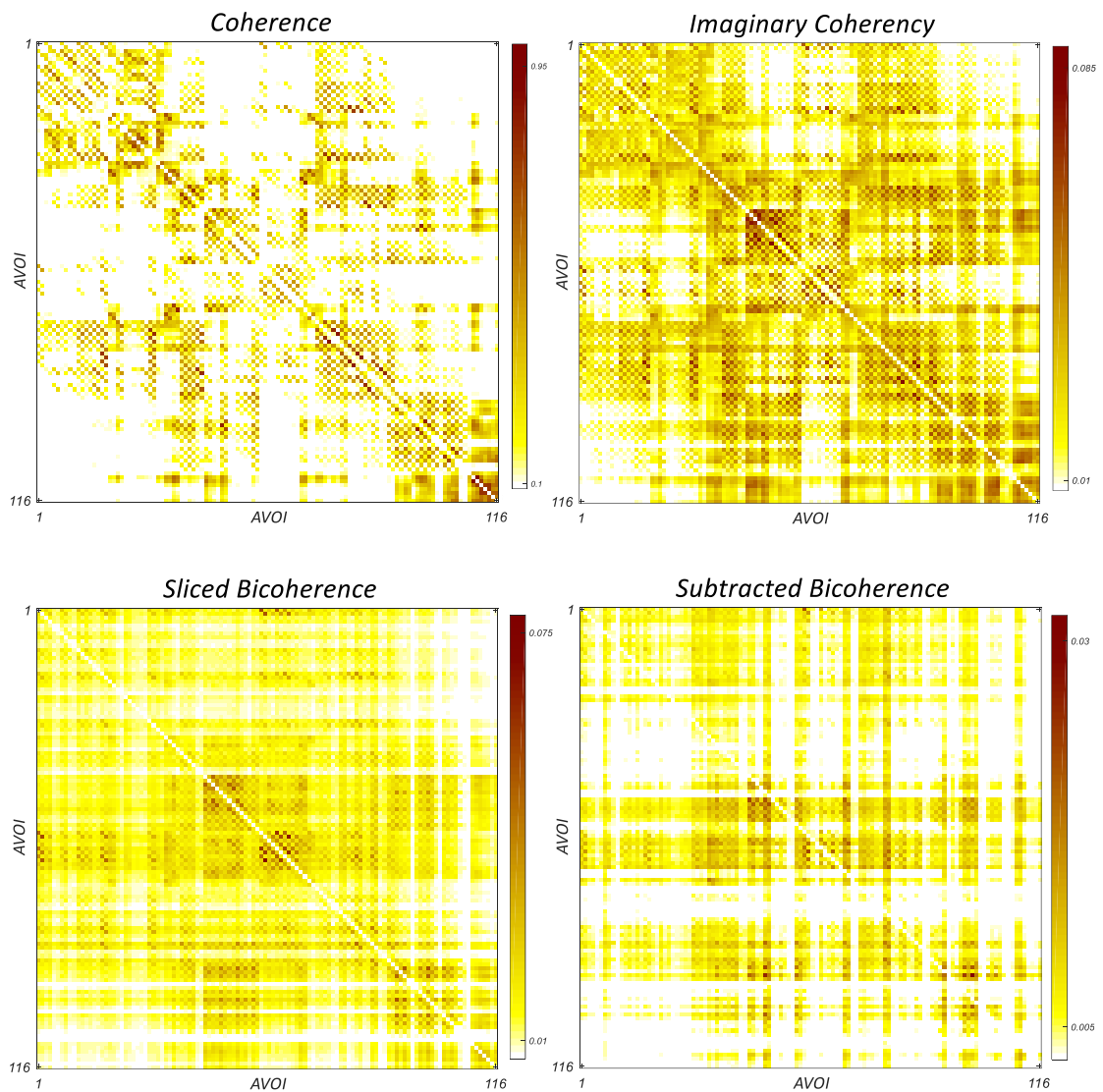
Alpha Band Connectivity Analysis

Figure 4.6 shows alpha band connectivity matrices for all methods. The matrices show interactions between different AVOIs. As expected for resting state data, all matrices show similar features indicating a strong connectivity between occipital regions (AVOIs 45-56) and the rest of the brain.

Figure 4.7 and Figure 4.8 show network level activity according to each metric. These figures are visualizations of connectivity matrices projected on a template brain. Each metric shows strong connectivity at the occipital regions of the brain with coherence and sliced bicoherence showing connectivity spreading all over the brain. On the other hand, imaginary coherency and subtracted bicoherence show localized activity around occipital regions.

Seed Based Connectivity Analysis

Figure 4.9 and Figure 4.10 show seed based connectivity results for all metrics. Because of its known role in resting state, Posterior Cingulate Cortex (PCC) is chosen as the seed. As expected, strong connectivity to parietal and occipital regions are found in all metrics. It is important to note that the regions around the seed show strong correlation in coherence and sliced bicoherence, which is not expected as a part of PCC network in resting state. These results is without doubt, the clearest evidence of volume conduction effect in coherence and sliced bicoherence. The robustness of imaginary coherency and subtracted bicoherence to volume conduction is also observed from seed based connectivity analysis.

Figure 4.6: Alpha Band Connectivity Results. Connectivity Measures. Coherence, Imaginary Alpha Band (8-12 Hz.) connectivity analysis on reduced virtual time series at 116 AVOI for each metric is carried out. Color bars indicate actual connectivity results averaged over 89 subjects. Coherence and Imaginary Coherency are symmetric measures; e.g. AVOI 1 $\rightarrow$ AVOI 2 = AVOI 2 $\rightarrow$ AVOI 1. Bicoherence based measures are non-symmetric. All metrics show high connectivity results around occipital regions as expected at resting state (see Appendix A).
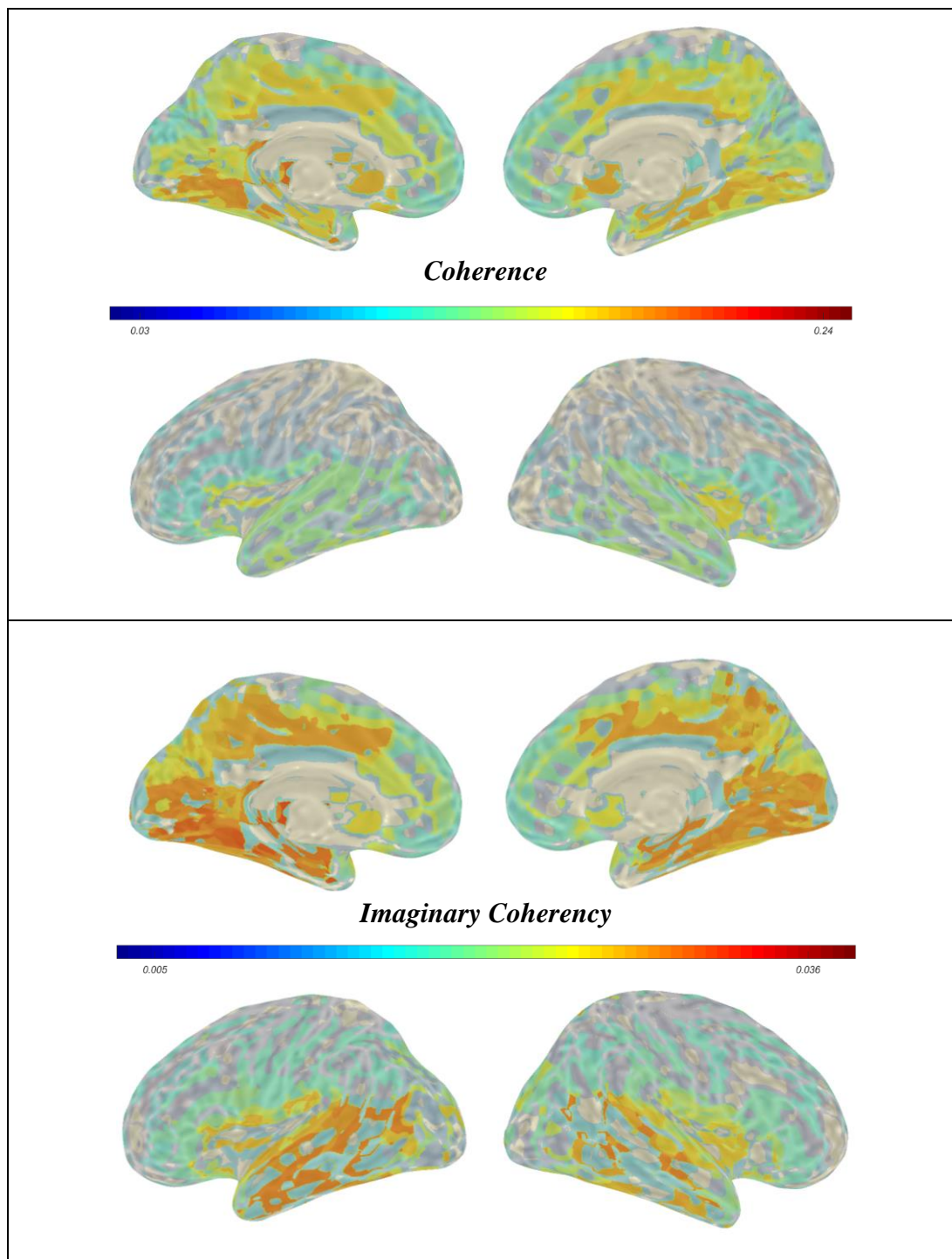
Figure 4.7: Network Degrees for Coherence and Imaginary Coherency. The degree of connection between AVOIs are projected to a template brain. AVOIs with most connectivity to other AVOIs are seen clearly from the scale. Note high connectivity results spreading all over the brain for Coherence. Connectivity results for Imaginary Coherency show more localized activity.
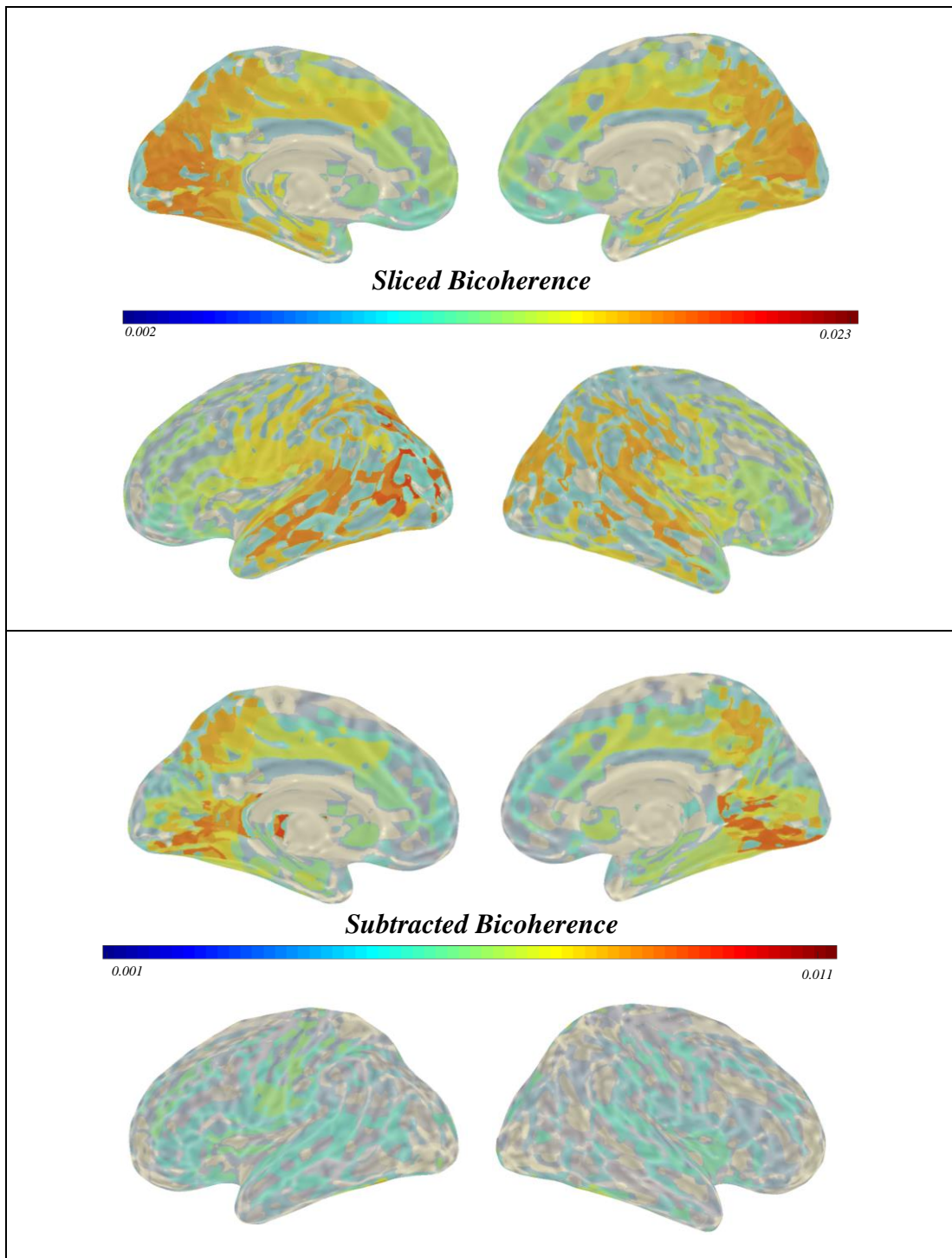
Figure 4.8: Network Degrees for Sliced Bicoherence and Subtracted Bicoherence. The degree of connection between AVOIs are projected to a template brain. AVOIs with most connectivity to other AVOIs are seen clearly from the scale. Similar high and spreading connectivity patterns are observed for Sliced Bicoherence. Subtracted Bicoherence results show robustness to volume conduction.
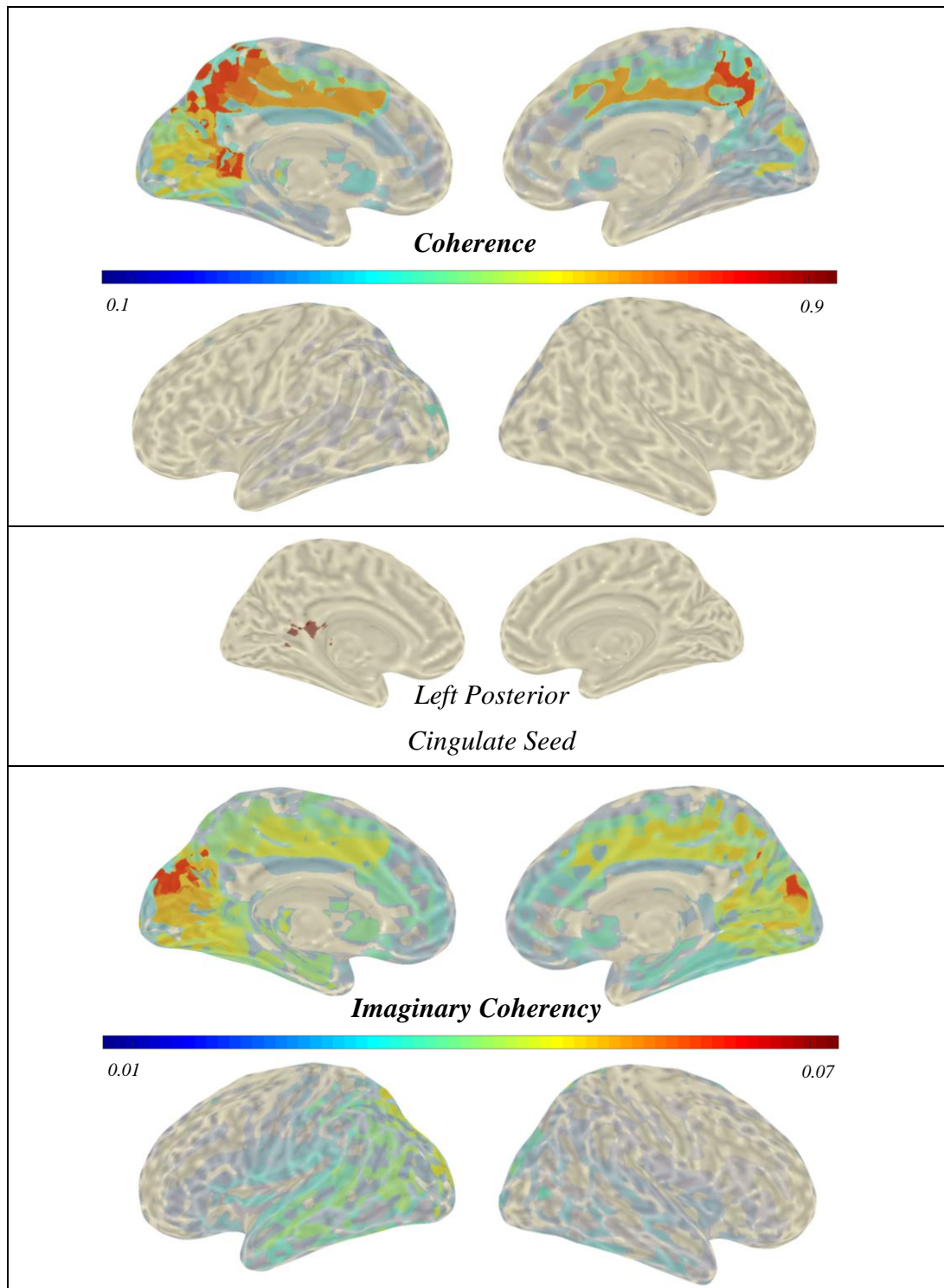
Figure 4.9: Seed Based Connectivity Analysis for Linear Methods. PCC seed is used for seed based connectivity analysis. Earlier resting state analysis show connectivity patterns between PCC, parietal and occipital regions. Coherence results show strong connectivity around the seed, indicating high volume conduction.
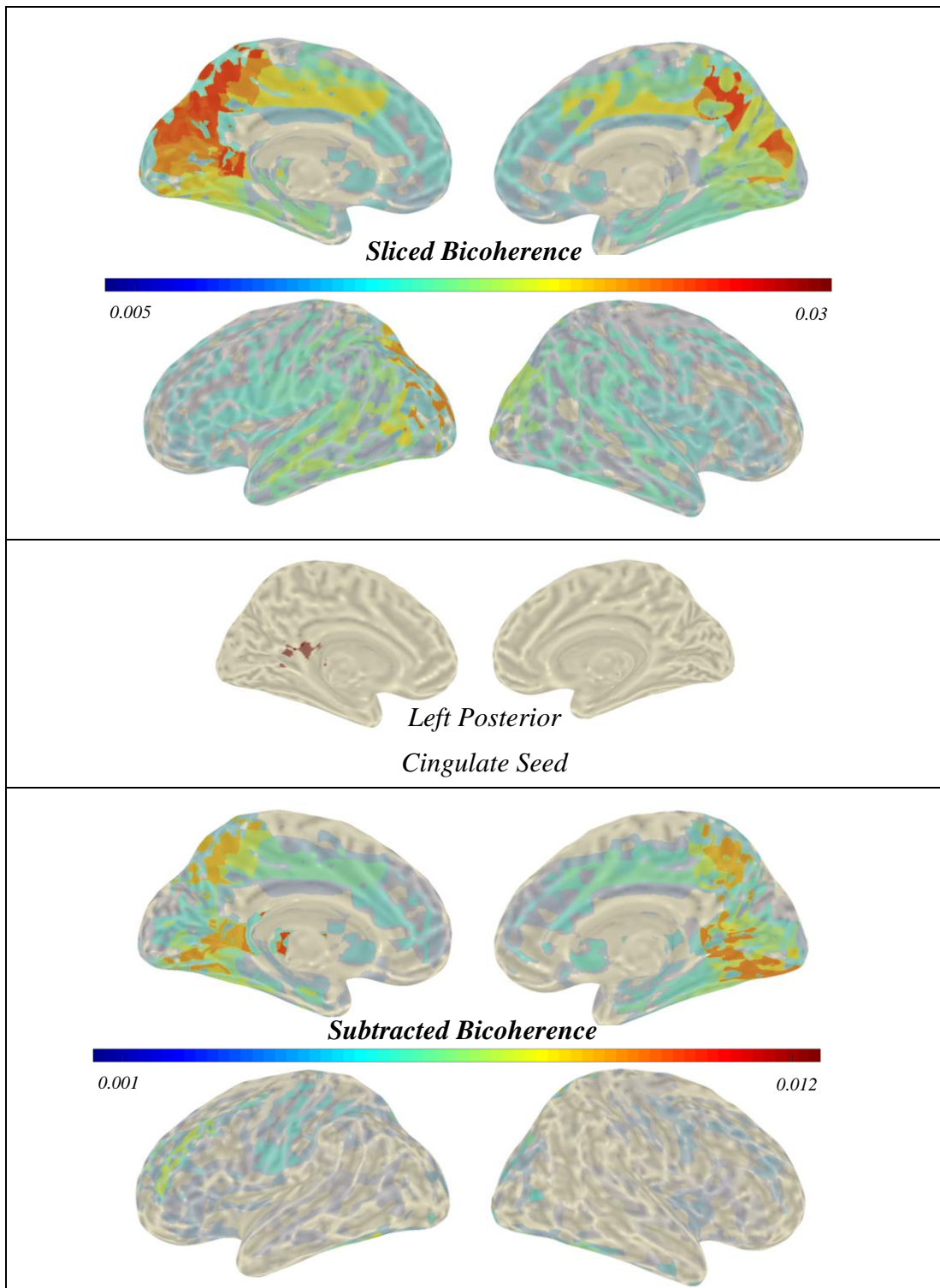
Figure 4.10: Seed Based Connectivity Analysis for Nonlinear Methods. PCC seed is used for seed based connectivity analysis. Similar to Coherence, Sliced Bicoherence show strong connectivity around the seed, indicating high volume conduction.

Between Metrics Correlation Analysis

Correlation results between each metric are given below. The percentage of significantly correlated AVOIs to total number of AVOIs is also provided per each comparison. It is important to note that occipital (45-56) and parietal (57-70) regions show similar results between each pair (see Appendix A). Also, the results of deep brain structures (regions between 37-42, 70-80 and 91-116) may be creating false results due to spatial resolution of MEG imaging (See Appendix A).
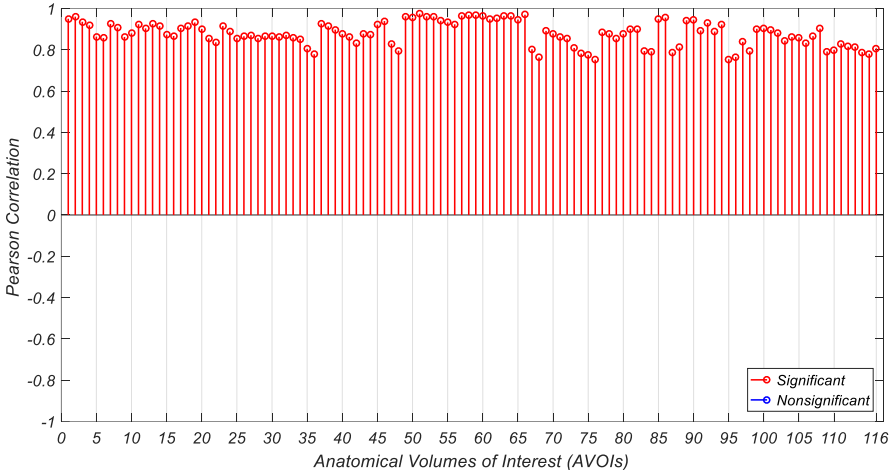
Figure 4.11: Correlation Analysis: Coherence – Imaginary Coherence. Significant and nonsignificant correlations are shown in different colors. Strong correlations between every AVOIs are observed.
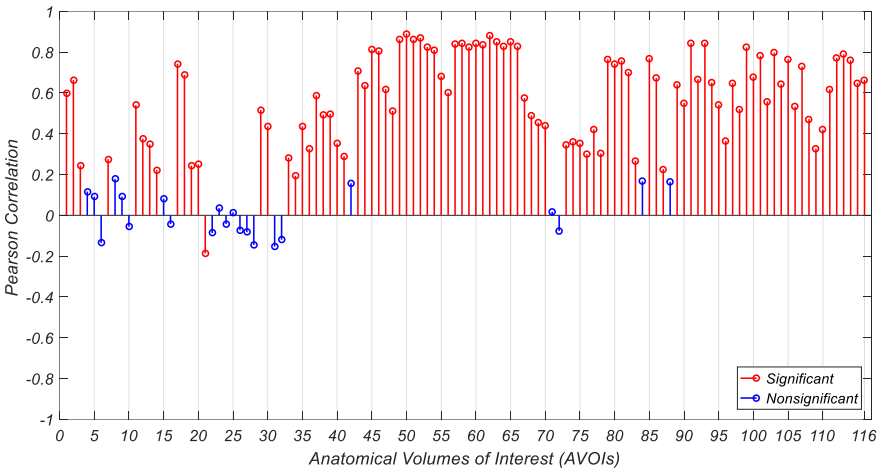
Figure 4.12: Correlation Analysis: Coherence - Sliced Bicoherence. Significant and nonsignificant correlations are shown in different colors. Strong correlations between most AVOIs are observed. AVOIs of occipital (45-56) and parietal (57-70) regions show consistent correlation in particular. The percentage of significantly correlated AVOIs to total number of AVOIs is 81%.

36
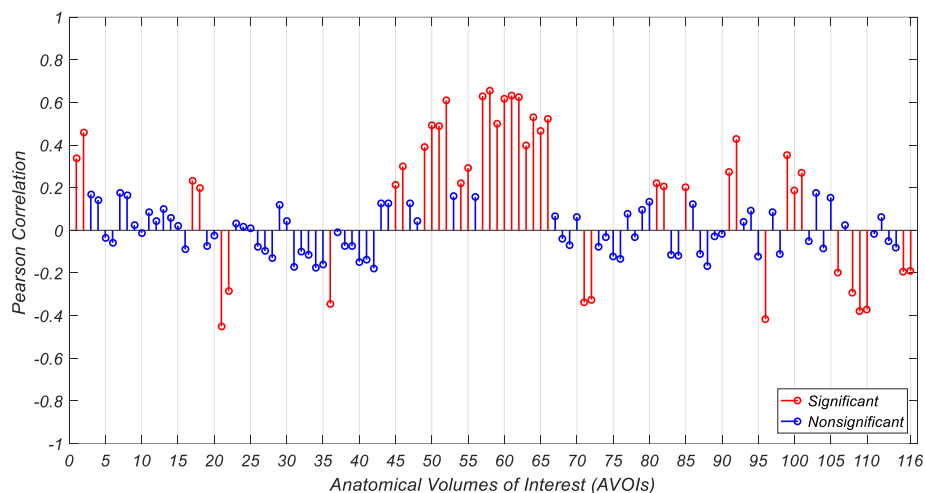
Figure 4.13: Correlation Analysis: Coherence - Subtracted Bicoherence. Significant and nonsignificant correlations are shown in different colors. Consistent correlations are only observed at parietal (57-70) regions. The percentage of significantly correlated AVOIs to total number of AVOIs is 36%.

Figure 4.14: Correlation Analysis: Imaginary Coherency - Sliced Bicoherence. Significant and nonsignificant correlations are shown in different colors. Strong correlations between most AVOIs are observed. The percentage of significantly correlated AVOIs to total number of AVOIs is 89%.

Figure 4.15: Correlation Analysis: Imaginary Coherency - Subtracted Bicoherence. Significant and nonsignificant correlations are shown in different colors. High correlation is observed at AVOIs of occipital (45-56) and parietal (57-70) regions. The percentage of significantly correlated AVOIs to total number of AVOIs is 46%.
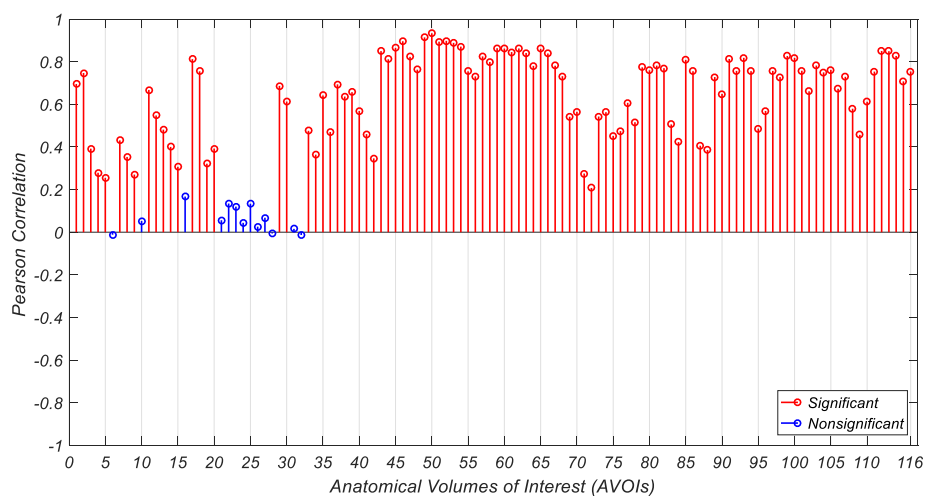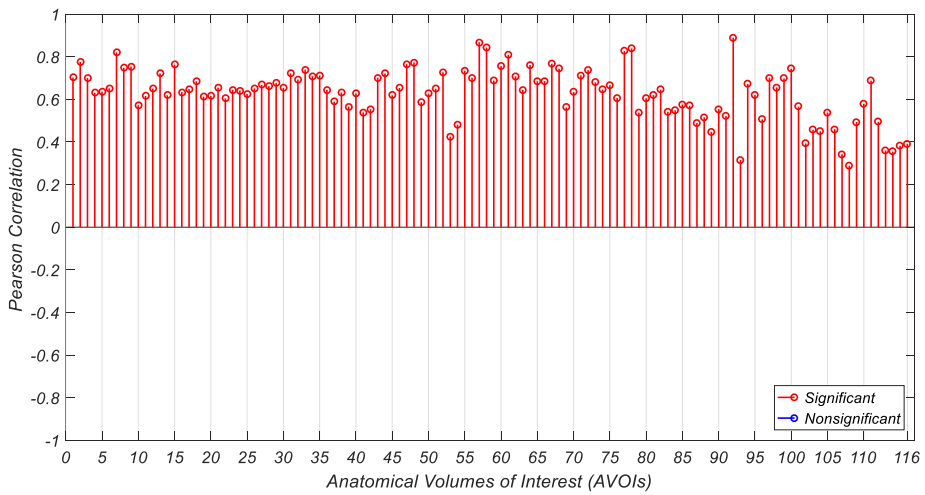

Figure 4.16: Correlation Analysis: Sliced Bicoherence - Subtracted Bicoherence. Significant and nonsignificant correlations are shown in different colors. Strong correlations between every AVOIs are observed.
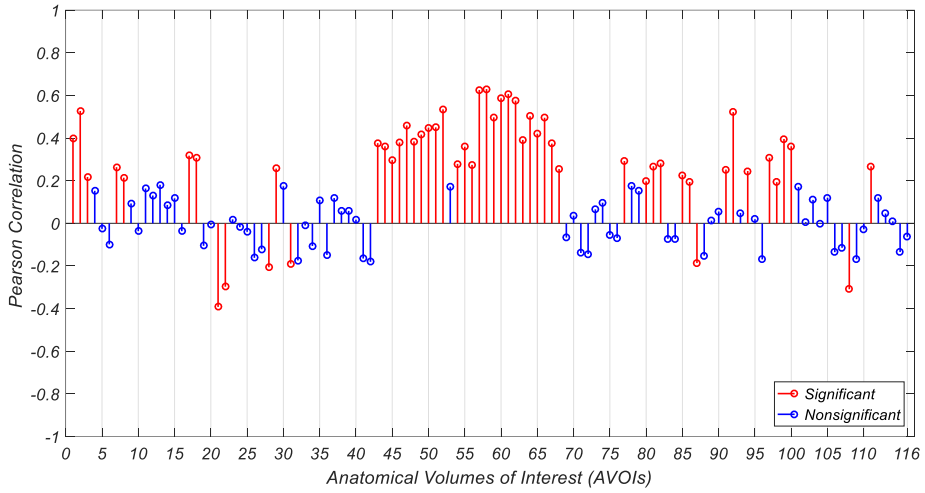
Between Metrics Reliability Analysis

Finally, we analyzed the group level reliability of each metric. Figure 4.17 shows that each metric have similar high reliability result meaning that all results are reproducible and repeatable across different subjects.
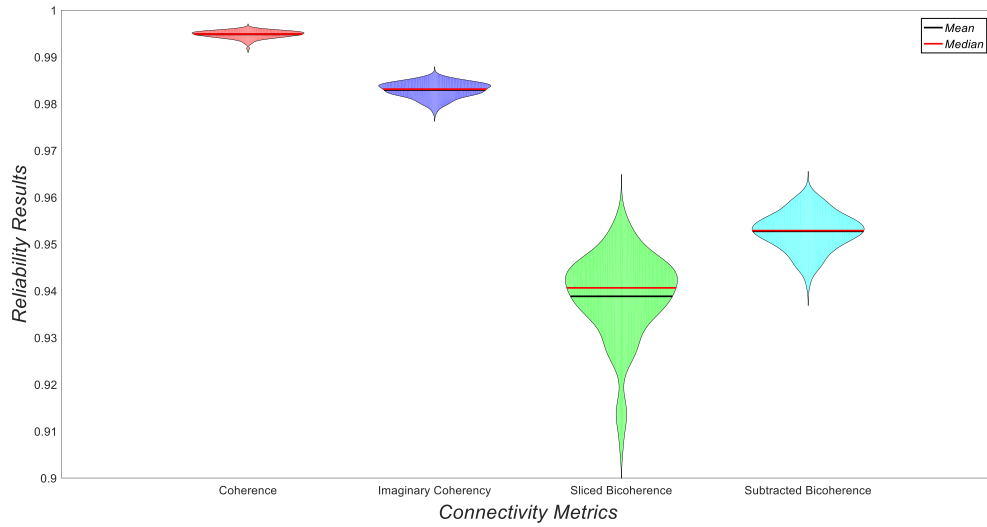
Figure 4.17: Split Half Reliability Test. All metrics show similar high reliability results meaning that the results are reproducible and repeatable.

CHAPTER 5

DISCUSSION AND CONCLUSION

5.1   Discussion

Our thesis is divided into two parts. In the first part, we hypothesized that the most prominent nonlinear interaction, particularly QPC, within the brain is concentrated at the slice of $f_1 = f_2 = f$ which implies coupling for $f_2 = 2f_1$. In order to test our hypothesis, we used higher order spectral analysis, namely bicoherence. Cross frequency coupling of $f_2 = 2f_1$ is actually visual at $f_2 = f_1$ coupling on bicoherence matrix (3.3). Thus, the main diagonal, also known as sliced bicoherence, where $f_2 = f_1$ is of interest within the study.

In the second part of the study, we compared nonlinear metrics with linear metrics in means of information content, commonality, volume conduction and reliability. We used 'sliced bicoherence' and 'subtracted bicoherence' (Özkurt T. E., 2016) as nonlinear metrics and 'coherence' and 'imaginary coherency' as linear metrics.

Earlier studies on bicoherence detected neural interactions particularly on the main diagonal. For example, a study on monkeys performing visuomotor tasks showed peaks at beta band on main diagonal of the bicoherence matrix (Wang, Chen, & Ding, 2007). In a resting state analysis, (Chella, Marzetti, Pizzella, Zappasodi, & Nolte, 2014) found significant peaks at alpha band. Similarly, (10-10 Hz.) coupling was identified by (Shahbazi, Ewald, & Nolte, 2014) at resting state data. Nevertheless, none of the studies investigated the information content of the sliced bicoherence comparatively. This study implements a statistical analysis method to compare diagonal and non-diagonal components of the bicoherence matrix.

Results of the study confirmed our hypothesis that the most prominent nonlinear interactions, particularly QPC is found on the main diagonal of the bicoherence matrix. We observed peaks on main diagonal at alpha band where $f_1 = f_2$, indicating a true interaction at $f_2 = 2f_1$ (3.3) (Figure 4.1). We also tested the same phenomenon for different anatomical volumes of interest. We found out that each and every region follows the same pattern, having the most important interactions at the main diagonal. Surely, this does not suggest that the non-diagonal components should be ignored.

Within the scope of this study, we also compared sliced and subtracted bicoherence to absolute and imaginary coherence. Our results showed that these share similar patterns for alpha band during resting state. Seed based connectivity analysis demonstrated specifically the robustness of imaginary coherency and subtracted bicoherence to volume conduction problem.

We compared information content of all metrics by correlating average connectivity metrics. In this manner, we compared coherence to sliced bicoherence and imaginary coherency to subtracted bicoherence. Results showed that there is a strong correlation between coherence and sliced bicoherence with 81%. On the other hand, 46% correlation was observed between imaginary coherency and subtracted bicoherence. Correlations between imaginary coherency and subtracted bicoherence is mostly concentrated at the occipital and the parietal regions.

Finally, our results suggest that all metrics show similar reliability results. This implies that the results are reproducible for different subjects.

To sum up, our results show that sliced bicoherence is a time efficient alternative to bicoherence estimation. Also, use of subtracted bicoherence to overcome volume conduction effect is favored.

5.2   Limitations

There are some limitations to this study. First of all, this study concentrates on resting state data. Task specific comparisons should also be carried in order to prove reliability and robustness of the metrics further. Also, comparison between linear and nonlinear metrics was only realized in the alpha band. Interactions at other bands should also be evaluated.

Another limitation of the study is the frequency resolution. For our studies we used 4 Hz. resolution due to computational costs. Higher frequency resolution would yield finer bicoherence estimations.

Last but not least, same metrics should be evaluated with different beamforming and parcellation methods in order to evaluate robustness to volume conduction effects.

5.3   Conclusion

In conclusion, this study shows that the information content of nonlinear interactions, particularly QPC, significantly concentrates on the main diagonal of bicoherence matrix. This result means that QPC mostly occurs between $(f_1 - f_2)$ frequencies where $f_2 = 2f_1$. Taking this into consideration, one can overcome high computational cost of bicoherence by calculating only the sliced bicoherence. This study also confirms the robustness of subtracted bicoherence to volume conduction effect. High reliability of both subtracted bicoherence and sliced bicoherence make them valid alternatives for nonlinear interaction estimation metrics. This study supports the idea that sliced bicoherence and subtracted bicoherence should be added to the rich collection of brain connectivity metrics.

REFERENCES

Ahlfors, S., Han, J., Belliveau, J., & Hämäläinen, M. (2010). Sensitivity of MEG and EEG to Source Orientation. *Brain Topography, 23*(3), 227-232. doi:10.1007/s10548-010-0154-x

Aydore, S., Pantazis, D., & Leahy, R. (2013). A note on the phase locking value and its properties. *NeuroImage, 74*, 231-244. doi:https://doi.org/10.1016/j.neuroimage.2013.02.008

Baillet, S. (2014). Forward and Inverse Problems of MEG/EEG. In D. Jaeger, & R. Jung, *Encyclopedia of Computational Neuroscience* (pp. 1-8). Springer Reference. doi:10.1007/978-1-4614-7320-6_529-1

Baillet, S., Friston, K., & Oostenveld, R. (2011). Academic Software Applications for Electromagnetic Brain Mapping Using MEG and EEG. *Computational Intelligence and Neuroscience, 2011*, 4 pages. doi:doi:10.1155/2011/972050

Baillet, S., Mosher, J., & Leahy, R. (2001). Electromagnetic Brain Mapping. *IEEE Signal Processing Magazine, 18*(6), 14-30. doi:10.1109/79.962275

Bandettini, P., Wong, E., Hinks, R., Tikofsky, R., & Hyde, J. (1992). Time course EPI of human brain function during task activation. *Magnetic Resonance in Medicine, 25*(2), 390-397. doi:10.1002/mrm.1910250220

Barnett, T., Johnson, L., Naitoh, P., Hicks, N., & Nute, C. (1971). Bispectrum Analysis of Electroencephalogram Signals during Waking and Sleeping. *Science, 172*(3981), 401-402. doi:10.1126/science.172.3981.401

Berger, H. (1929). Über das Elektrenkephalogramm des Menschen. *Archiv für Psychiatrie und Nervenkrankheiten, 87*(1), 527-570. doi:https://doi.org/10.1007/BF01797193

Breakspear, M., & Terry, J. (2002). Detection and description of non-linear interdependence in normal multichannel human EEG data. *Clinical Neurophysiology, 113*(5), 735-753. doi:https://doi.org/10.1016/S1388-2457(02)00051-2

Brodmann, K. (1909). Vergleichende Lokalisationslehre der Grosshirnrinde. *Leipzig: Johann Ambrosius Barth*.

Brookes, M., Hale, J., Zumer, J., Stevenson, C., Francis, S., & Gareth, R. (2011). Measuring functional connectivity using MEG: Methodology and comparison

with fcMRI. *NeuroImage, 56*(3), 1082-1104. doi:http://doi.org/10.1016/j.neuroimage.2011.02.054

Chella, F., Marzetti, L., Pizzella, V., Zappasodi, F., & Nolte, G. (2014). Third order spectral analysis robust to mixing artifacts for mapping cross-frequency interactions in EEG/MEG. *NeuroImage, 91*, 146-161. doi:https://doi.org/10.1016/j.neuroimage.2013.12.064

Cohen, D. (1968). Magnetoencephalography: Evidence of Magnetic Fields Produced by Alpha-Rhythm Currents. *Science, 161*(3843), 784-786. doi:10.1126/science.161.3843.784

Cohen, D. (1970). Large-volume conventional magnetic shields. *Revue de Physique Appliquée, 5*, 53-58.

Cohen, M. X. (2014). *Analyzing neural time series data: theory and practice.* MIT Press.

Colclough, G., Woolrich, M., Tewarie, P., Brookes, M., Quinn, A., & Smith, S. (2016). How reliable are MEG resting-state connectivity metrics? *NeuroImage, 138*, 284-293. doi:https://doi.org/10.1016/j.neuroimage.2016.05.070

David, O., Cosmelli, D., & Friston, K. (2003). Evaluation of different measures of functional connectivity using a neural mass model. *NeuroImage, 21*(2004), 659-673. doi:10.1016/j.neuroimage.2003.10.006

Domínguez, L., Stieben, J., Pérez Velázquez, J., & Shanker, S. (2013). The imaginary part of coherency in autism: differences in cortical functional connectivity in preschool children. *PLoS ONE, 8*(10), e75941. doi:https://doi.org/10.1371/journal.pone.0075941

Drakesmith, M., El-Deredy, W., & Welbourne, S. (2013). Reconstructing coherent networks from electroencephalography and magnetoencephalography with reduced contamination from volume conduction or magnetic field spread. *PLoS One, 8*(12), e81553. doi:doi:10.1371/journal.pone.0081553

Duda, J. (2010). *Characterizing Connectivity in Brain Networks.* Publicly Accessible Penn Dissertations. Retrieved from https://repository.upenn.edu/edissertations/191

Dumermuth, G., Huber, P., Kleiner, B., & Gasser, T. (1971). Analysis of the interrelations between frequency bands of the EEG by means of the bispectrum a preliminary study. *Electroencephalography and Clinical Neurophysiology, 31*(2), 137-148. doi:https://doi.org/10.1016/0013-4694(71)90183-0

Efron, B. (1979). *Bootstrap Methods: Another Look at the Jackknife.* Stanford University.

Elgar, S., Van Atta, C., & Gharib, M. (1990). Cross-bispectral analysis of a vibrating cylinder and its wake in low Reynolds number flow. *Journal of Fluids and Structures, 4*(1), 59-71. doi:https://doi.org/10.1016/0889-9746(90)90043-5

Feldman, R. P., & Goodrich, J. T. (1999). The Edwin Smith Surgical Papyrus. *Child's Nervous System, 15*, 281-284.

Feynman, R., Leighton, R., & Sands, M. (1964). *The Feynman Lectures on Physics.* Addison–Wesley.

Finger, S. (2000). *Minds Behind the Brain: A History of the Pioneers and Their Discoveries.* Oxford University Press.

Florin, E., & Baillet, S. (2015). The brain's resting-state activity is shaped by synchronized cross-frequency coupling of neural oscillations. *NeuroImage, 111*, 26-35. doi:https://doi.org/10.1016/j.neuroimage.2015.01.054

Freemon, F. R. (1994). Galen's ideas on neurological function. *Journal of the History of the Neurosciences, 3*(4), 263-271.

Fries, P. (2005). A mechanism for cognitive dynamics: neuronal communication through neuronal coherence. *Trends in Cognitive Science, 9*(10), 474-480.

Friston, K. (2011). Functional and effective connectivity: a review. *Brain Connectivity, 1*(1), 13-36. doi:10.1089/brain.2011.0008

Friston, K. J. (1994). Functional and effective connectivity in neuroimaging: A synthesis. *Human Brain Mapping, 2*(1-2), 56-78. doi:10.1002/hbm.460020107

Garcia-Lopez, P., Garcia-Marin, V., & Freire, M. (2010). The histological slides and drawings of Cajal. *Frontiers in Neuroanatomy, 4*. doi:10.3389/neuro.05.009.2010

Garey , L. (2006). *Brodmann's Localisation in the Cerebral Cortex.* (L. Garey, Trans.) Springer US. doi:10.1007/b138298

Glover, G. H. (2011). Overview of Functional Magnetic Resonance Imaging. *Neurosurgery Clinics of North America, 22*(2), 133-139. doi:10.1016/j.nec.2010.11.001

Gomez-Herrero, G. (2010). *Brain Connectivity Analysis with EEG.* Tampere University of Technology.

Gross, C. G. (1987). *Early History of Neuroscience.* Boston: Encylopedia of Neuroscience.

Gross, J., Kujala, j., Hamalainen, M., Timmermann, L., Schnitzler, A., & Salmelin, R. (2001). Dynamic imaging of coherent sources: Studying neural interactions in the human brain. *Proceedings of the National Academy of Sciences of the United States of America, 98*(2), 694-699. doi:10.1073/pnas.98.2.694

Haas, L. (2003). Hans Berger (1873–1941), Richard Caton (1842–1926), and electroencephalography. *J Neurol Neurosurg Psychiatry, 74*(1), 9. doi:http://dx.doi.org/10.1136/jnnp.74.1.9

Hagmann, P., Cammoun, L., Gigandet, X., Meuli, R., Honey, C. J., Wedeen, V., & Sporns, O. (2008). Mapping the Structural Core of Human Cerebral Cortex. *PLoS Biology, 6*(7), 159. doi:https://doi.org/10.1371/journal.pbio.0060159

Hämäläinen, M., Hari, R., Ilmoniemi, R., Knuutila, J., & Lounasmaa, O. (1993). Magnetoencephalography—theory, instrumentation, and applications to noninvasive studies of the working human brain. *Reviews of Modern Physics, 65*(2), 413. doi:https://doi.org/10.1103/RevModPhys.65.413

Hansen, P., Kringelbach, M., & Salmelin, R. (2010). *MEG: An Introduction to Methods.* Oxford University Press.

Hari, R. (2011). Magnetoencephalography: Methods and applications. In D. Schomer, & F. Lopes da Silva, *Niedermeyer's Electroencephalography: Basic Principles, Clinical Applications and Related Fields (6th Edition)* (pp. 865-900). Philadelphia: Lippincott Williams & Wilkins.

He, B., Yang, L., Wilke, C., & Yuan, H. (2011). Electrophysiological Imaging of Brain Activity and Connectivity—Challenges and Opportunities. *IEEE Transactions on Biomedical Engineering, 58*(7), 1918-1931. doi:10.1109/TBME.2011.2139210

Hohlefeld, F., Huchzermeyer, C., Huebl, J., Schneider, G., Nolte, G., Brücke, C., . . . Nikulin, V. (2013). Functional and effective connectivity in subthalamic local field potential recordings of patients with Parkinson's disease. *Neuroscience, 250*, 320-332. doi:10.1016/j.neuroscience.2013.07.028

Huang, M., Mosher, J., & Leahy, R. (1999). A sensor-weighted overlapping-sphere head model and exhaustive head model comparison for MEG. *Physics in Medicine and Biology, 44*(2), 423-440.

Isler, J., Grieve, P., Czernochowski, D., Stark, R., & Friedman, D. (2008). Cross-frequency phase coupling of brain rhythms during the orienting response. *Brain Research, 1232*, 163-172. doi:10.1016/j.brainres.2008.07.030

Jirsa, V., & Müller, V. (2013). Cross-frequency coupling in real and virtual brain networks. *Frontiers in Computational Neuroscience, 7*, 78. doi:https://doi.org/10.3389/fncom.2013.00078

Kirschstein, T., & Köhling, R. (2009). What is the Source of the EEG? *Clinical EEG and Neuroscience, 40*(3), 29-37. doi:https://doi.org/10.1177/155005940904000305

Kwong, K., Belliveau, J., Chesler, D., Goldberg, I., Weisskoff, R., Poncelet, B., . . . Turner, R. (1992). Dynamic magnetic resonance imaging of human brain activity during primary sensory stimulation. *Proceedings of the National Academy of Sciences of the United States of America, 89*(12), 5675-5679. doi:https://doi.org/10.1073/pnas.89.12.5675

Lemieux, L., Daunizeau, J., & Walker, M. (2011). Concepts of connectivity and human epileptic activity. *Frontiers in Systems Neuroscience.* doi:https://doi.org/10.3389/fnsys.2011.00012

Liu, Z., Ding, L., & He, B. (2006). Integration of EEG/MEG with MRI and fMRI in Functional Neuroimaging. *IEEE engineering in medicine and biology magazine : the quarterly magazine of the Engineering in Medicine & Biology Society, 25*(4), 46-53.

López-Muñoz, F., Boya, J., & Alamo, C. (2006). Neuron theory, the cornerstone of neuroscience, on the centenary of the Nobel Prize award to Santiago Ramón y Cajal. *Brain Research Bulletin, 70*(4-6), 391-405. doi:https://doi.org/10.1016/j.brainresbull.2006.07.010

Marin, G., Guérin, C., Baillet, S., Meunier, G., & Meunier, G. (1998). Influence of skull anisotropy for the forward and inverse problem in EEG: Simulation studies using FEM on realistic head models. *Human Brain Mapping, 6*(4), 250-269. doi:10.1002/(SICI)1097-0193(1998)6:4<250::AID-HBM5>3.0.CO;2-2

Mohamed, W. M. (2008). The Edwin Smith Surgical Papyrus: Neuroscience in Ancient Egypt. *IBRO Reports.*

Mosher, J., Leahy, R., & Lewis, P. (1999). EEG and MEG: forward solutions for inverse methods. *IEEE Transactions on Biomedical Engineering, 46*(3), 245-259.

Nikias, C., & Mendel, J. (1993). Signal processing with higher-order spectra. *IEEE Signal Processing Magazine, 10*(3), 10-37. doi:10.1109/79.221324

Nolte, G., Bai, O., Wheaton, L., Mari, Z., Vorbach, S., & Hallett, M. (2004). Identifying true brain interaction from EEG data using the imaginary part of coherency. *Clinical Neurophysiology, 115*(2004), 2292-2307. doi:10.1016/j.clinph.2004.04.029

Nunez, P., & Srinivasan, R. (2006). *Electric Fields of the Brain: The Neurophysics of EEG.* Oxford University Press.

Nunezab, P., Srinivasanbc, R., Westdorpad, A., Wijesingheag, R., Tuckerbc, D., Silbersteinef, R., & Caduschef, P. (1997). EEG coherency: I: statistics, reference electrode, volume conduction, Laplacians, cortical imaging, and interpretation at multiple scales. *Electroencephalography and Clinical Neurophysiology, 103*(5), 499-515. doi:https://doi.org/10.1016/S0013-4694(97)00066-7

Ogawa, S., Tank, D., Menon, R., Ellermann, J., Kim, S., Merkle, H., & Ugurbil, K. (1992). Intrinsic signal changes accompanying sensory stimulation: functional brain mapping with magnetic resonance imaging. *Proceedings of the National Academy of Sciences of the United States of America, 89*(13), 5951-5955.

Oostenveld, R., Fries, P., Maris, E., & Schoffelen, J.-M. (2011). FieldTrip: Open Source Software for Advanced Analysis of MEG, EEG, and Invasive Electrophysiological Data. *Computational Intelligence and Neuroscience, 2011*. doi:http://dx.doi.org/10.1155/2011/156869

Özkurt, T. E. (2016). Estimation of nonlinear neural source interactions via sliced bicoherence. *Biomedical Signal Processing and Control, 30*, 43-52. doi:https://doi.org/10.1016/j.bspc.2016.05.001

Özkurt, T. E., & Schnitzler, A. (2011). A critical note on the definition of phase–amplitude cross-frequency coupling. *Journal of Neuroscience Methods, 201*(2), 438-443. doi:https://doi.org/10.1016/j.jneumeth.2011.08.014

Palva, S., & Palva, J. (2012). Discovering oscillatory interaction networks with M/EEG: challenges and breakthroughs. *Trends in Cognitive Sciences, 16*(4), 219-230. doi:https://doi.org/10.1016/j.tics.2012.02.004

Pauling, L., & Coryell, C. (1936). The Magnetic Properties and Structure of Hemoglobin, Oxyhemoglobin and Carbonmonoxyhemoglobin. *Proceedings of the National Academy of Sciences of the United States of America, 22*(4), 210-216.

Pawela, C., & Biswal, B. (2011). Brain Connectivity: A New Journal Emerges. *Brain Connectivity, 1*(1), 1-2. doi:10.1089/brain.2011.0020

Pereda, E., Quiroga, R., & Bhattacharya, J. (2005). Nonlinear multivariate analysis of neurophysiological signals. *77*(1-2), 1-37. doi:https://doi.org/10.1016/j.pneurobio.2005.10.003

Ramírez, R. R. (2008). Source localization. *Scholarpedia, 3*(11), 1733. doi:10.4249/scholarpedia.1733

Robinson, S., & Vrba, J. (1999). Functional neuroimaging by Synthetic Aperture Magnetometry (SAM). In *Recent Advances in Biomagnetism* (pp. 302-305). Tohoku University Press.

Sakkalis, V. (2011). Review of advanced techniques for the estimation of brain connectivity measured with EEG/MEG. *Computers Biology and Medicine, 41*(2011), 1110-1117. doi:10.1016/j.compbiomed.2011.06.020

Sampaio-Baptista, C., & Johansen-Berg, H. (2017). White Matter Plasticity in the Adult Brain. *Neuron, 96*(6), 1239-1251. doi:10.1016/j.neuron.2017.11.026

Sander, T., Bock, A., Leistner, S., Kühn, A., & Trahms, L. (2010). Coherence and imaginary part of coherency identifies cortico-muscular and cortico-thalamic coupling. *32nd Annual International Conference of the IEEE EMBS.* Buenos Aires.

Sarvas, J. (1987). Basic mathematical and electromagnetic concepts of the biomagnetic inverse problem. *Physics in Medicine & Biology, 32*(1), 11. Retrieved from http://stacks.iop.org/0031-9155/32/i=1/a=004

Schmidt, R. (1986). Multiple emitter location and signal parameter estimation. *IEEE Transactions on Antennas and Propagation, 34*(3), 276-280. doi:10.1109/TAP.1986.1143830

Schnitzler, A., & Gross, J. (2005). Normal and pathological oscillatory communication in the brain. *Nature Reviews Neuroscience, 6*, 285-296. doi:doi:10.1038/nrn1650

Schoffelen, J.-M., & Gross, J. (2009). Source connectivity analysis with MEG and EEG. *Human Brain Mapping*, 1857-1865. doi:http://dx.doi.org/10.1002/hbm.20745

Shahbazi, F., Ewald, A., & Nolte, G. (2014). Univariate normalization of bispectrum using Hölder's inequality. *Journal of Neuroscience Methods, 233*, 177-186. doi:https://doi.org/10.1016/j.jneumeth.2014.05.030

Sharon, D., Hämäläinen, M., Tootell, R., Halgren, E., & Belliveau, J. (2007). The advantage of combining MEG and EEG: comparison to fMRI in focally stimulated visual cortex. *NeuroImage, 36*(4), 1225-1235. doi:10.1016/j.neuroimage.2007.03.066

Siegel, M., Donner, T., & Engel, A. (2012). Spectral fingerprints of large-scale neuronal interactions. *Nature Reviews Neuroscience, 13*, 121-134. doi:doi:10.1038/nrn3137

Solin, A., Jylanki, P., Kauramaki, J., Heskes, T., Gerven, M., & Sarkka, S. (2016). Regularizing Solutions to the MEG Inverse Problem Using Space–Time Separable Covariance Functions. *arXiv preprint*, 1604.

Sporns, O. (2007). Brain Connectivity. *Scholarpedia, 2*(10), 4695.

Sporns, O., Tononi, G., & Kötter, R. (2005). The Human Connectome: A Structural Description of the Human Brain. *PLoS Computational Biology, 1*(4), 42. doi:https://doi.org/10.1371/journal.pcbi.0010042

Stam, C., Breakspear, M., van Walsum, A.-M., & van Dijk, B. (2003). Nonlinear synchronization in EEG and whole-head MEG recordings of healthy subjects. *Human Brain Mapping, 19*(2), 63-78. doi:10.1002/hbm.10106

Stenroos, M., & Sarvas, J. (2012). Bioelectromagnetic forward problem: isolated source approach revis(it)ed. *Physics in Medicine and Biology, 57*(11), 3517-3535. doi:10.1088/0031-9155/57/11/3517

Stinstra, J., & Peters, M. (1988). The volume conductor may act as a temporal filter on the ECG and EEG. *Medical & Biological Engineering & Computing, 36*(6), 711-716.

Swami, A., Mendel, J., & Nikias, C. (1993). *Higher-Order Spectral Analysis Toolbox.* United Signals & Systems, Inc.

Tanzer, I. O. (2006). *Numerical Modelling in Electro- and Magnetoencephalography.* Helsinki University of Technology.

Tononi, G., Sporns, O., & Edelman, G. (1994). A measure for brain complexity: relating functional segregation and integration in the nervous system. *Proceedings of the National Academy of Sciences, 91*(11), 5033-5037.

Tzourio-Mazoyer, N., Landeau, B., Papathanassiou, D., Crivello, F., & Etard, O. (2002). Automated anatomical labeling of activations in SPM using a macroscopic anatomical parcellation of the MNI MRI single-subject brain. *Neuroimage, 15*(1), 273-289. doi:10.1006/nimg.2001.0978

Van Essen, D., Smith, S., Barch, D., Behrens, T., Yacoub, E., Ugurbil, K., & WU-Minn HCP Consortium. (2013). The WU-Minn Human Connectome Project: an overview. *Neuroimage, 80*, 62-79. doi:10.1016/j.neuroimage.2013.05.041

Van Laere, J. (1993). Vesalius and the nervous system. *Verh K Acad Geneeskd Belg, 55*(6), 533-576.

Van Veen, B., van Drongelen, W., Yuchtman, M., & Suzuki, A. (1997). Localization of brain electrical activity via linearly constrained minimum variance spatial filtering. *IEEE Transactions on Bio-medical Engineering, 44*(9), 867-880. doi:10.1109/10.623056

Venkatakrishnan, P., Sukanesh, R., & Sangeetha, S. (2011). Detection of quadratic phase coupling from human EEG signals using higher order statistics and spectra. *Signal Image and Video Processing, 5*(2), 217-229. doi:10.1007/s11760-010-0156-x

Wallisch, P. (2014). Functional Magnetic Resonance Imaging. In P. Wallisch, M. Lusignan, M. Benayoun, T. Baker, A. Dickey, & N. Hatsopoulos, *MATLAB for Neuroscientists* (pp. 361-379). Academic Press.

Wang, X., Chen, Y., & Ding, M. (2007). Testing for Statistical Significance in Bispectra: A Surrogate Data Approach and Application to Neuroscience. *54*(11). doi:10.1109/TBME.2007.895751

WU-Minn HCP Consortium. (2017). *Human Connectome Project 1200 Subjects Data Release Reference Manual.*

Zimmerman, J., Thiene, P., & Harding, J. (1970). Design and Operation of Stable rf-Biased Superconducting Point-Contact Quantum Devices, and a Note on the Properties of Perfectly Clean Metal Contacts. *Journal of Applied Physics, 41*(4), 1572. doi:https://doi.org/10.1063/1.1659074

APPENDIX A

ANATOMICAL VOLUMES OF INTEREST LABELS

1	'Precentral_L'	59	'Parietal_Sup_L'
2	'Precentral_R'	60	'Parietal_Sup_R'
3	'Frontal_Sup_L'	61	'Parietal_Inf_L'
4	'Frontal_Sup_R'	62	'Parietal_Inf_R'
5	'Frontal_Sup_Orb_L'	63	'SupraMarginal_L'
6	'Frontal_Sup_Orb_R'	64	'SupraMarginal_R'
7	'Frontal_Mid_L'	65	'Angular_L'
8	'Frontal_Mid_R'	66	'Angular_R'
9	'Frontal_Mid_Orb_L'	67	'Precuneus_L'
10	'Frontal_Mid_Orb_R'	68	'Precuneus_R'
11	'Frontal_Inf_Oper_L'	69	'Paracentral_Lobule_L'
12	'Frontal_Inf_Oper_R'	70	'Paracentral_Lobule_R'
13	'Frontal_Inf_Tri_L'	71	'Caudate_L'
14	'Frontal_Inf_Tri_R'	72	'Caudate_R'
15	'Frontal_Inf_Orb_L'	73	'Putamen_L'
16	'Frontal_Inf_Orb_R'	74	'Putamen_R'
17	'Rolandic_Oper_L'	75	'Pallidum_L'
18	'Rolandic_Oper_R'	76	'Pallidum_R'
19	'Supp_Motor_Area_L'	77	'Thalamus_L'
20	'Supp_Motor_Area_R'	78	'Thalamus_R'
21	'Olfactory_L'	79	'Heschl_L'
22	'Olfactory_R'	80	'Heschl_R'
23	'Frontal_Sup_Medial_L'	81	'Temporal_Sup_L'
24	'Frontal_Sup_Medial_R'	82	'Temporal_Sup_R'
25	'Frontal_Med_Orb_L'	83	'Temporal_Pole_Sup_L'
26	'Frontal_Med_Orb_R'	84	'Temporal_Pole_Sup_R'
27	'Rectus_L'	85	'Temporal_Mid_L'
28	'Rectus_R'	86	'Temporal_Mid_R'
29	'Insula_L'	87	'Temporal_Pole_Mid_L'
30	'Insula_R'	88	'Temporal_Pole_Mid_R'
31	'Cingulum_Ant_L'	89	'Temporal_Inf_L'
32	'Cingulum_Ant_R'	90	'Temporal_Inf_R'
33	'Cingulum_Mid_L'	91	'Cerebelum_Crus1_L'
34	'Cingulum_Mid_R'	92	'Cerebelum_Crus1_R'
35	'Cingulum_Post_L'	93	'Cerebelum_Crus2_L'
36	'Cingulum_Post_R'	94	'Cerebelum_Crus2_R'
37	'Hippocampus_L'	95	'Cerebelum_3_L'

38	'Hippocampus_R'	96	'Cerebelum_3_R'
39	'ParaHippocampal_L'	97	'Cerebelum_4_5_L'
40	'ParaHippocampal_R'	98	'Cerebelum_4_5_R'
41	'Amygdala_L'	99	'Cerebelum_6_L'
42	'Amygdala_R'	100	'Cerebelum_6_R'
43	'Calcarine_L'	101	'Cerebelum_7b_L'
44	'Calcarine_R'	102	'Cerebelum_7b_R'
45	'Cuneus_L'	103	'Cerebelum_8_L'
46	'Cuneus_R'	104	'Cerebelum_8_R'
47	'Lingual_L'	105	'Cerebelum_9_L'
48	'Lingual_R'	106	'Cerebelum_9_R'
49	'Occipital_Sup_L'	107	'Cerebelum_10_L'
50	'Occipital_Sup_R'	108	'Cerebelum_10_R'
51	'Occipital_Mid_L'	109	'Vermis_1_2'
52	'Occipital_Mid_R'	110	'Vermis_3'
53	'Occipital_Inf_L'	111	'Vermis_4_5'
54	'Occipital_Inf_R'	112	'Vermis_6'
55	'Fusiform_L'	113	'Vermis_7'
56	'Fusiform_R'	114	'Vermis_8'
57	'Postcentral_L'	115	'Vermis_9'
58	'Postcentral_R'	116	'Vermis_10'